Larkin, Cormac J.K.; Lundén, Ville; Schulz, Leonard; Baumgartner-Steinleitner, Markus; Brekkum, Marianne; Dazzi, Pietro; Cegla, Adam; Iuliis, Alessia De; Gesch, Jonas; Lennerstrand, Sofia; Nesbit-Östman, Sara; Pires, Vasco D.C.; Palanca, Inés Terraza; Teubenbacher, Daniel; Enengl, Florine; Hallmann, Marcus

M^5 — Mars Magnetospheric Multipoint Measurement Mission: A multi-spacecraft plasma physics mission to Mars

Published in:
Advances in Space Research

DOI:
10.1016/j.asr.2023.11.032

Published: 15/03/2024

Document Version
Publisher's PDF, also known as Version of record

Available online at www.sciencedirect.com

ScienceDirect

Advances in Space Research 73 (2024) 3235–3255

ADVANCES IN SPACE RESEARCH (a COSPAR publication)

www.elsevier.com/locate/asr

M^5 — Mars Magnetospheric Multipoint Measurement Mission: A multi-spacecraft plasma physics mission to Mars

Cormac J.K. Larkin [a,b,c,d,*], Ville Lundén [e], Leonard Schulz [f], Markus Baumgartner-Steinleitner [g], Marianne Brekkum [h], Adam Cegla [i], Pietro Dazzi [j,k], Alessia De Iuliis [l], Jonas Gesch [m], Sofia Lennerstrand [n], Sara Nesbit-Östman [o], Vasco D.C. Pires [p], Inés Terraza Palanca [q], Daniel Teubenbacher [r,s], Florine Enengl [t], Marcus Hallmann [u]

[a] *Zentrum für Astronomie der Universität Heidelberg, Astronomisches Rechen-Institut, Mönchhofstr. 12-14, 69120 Heidelberg, Germany*
[b] *Max-Planck-Institut für Kernphysik, Saupfercheckweg 1, 69117 Heidelberg, Germany*
[c] *Max-Planck-Institut für Astronomie, Königstuhl 17, D-69117 Heidelberg, Germany*
[d] *Kapteyn Astronomical Institute, University of Groningen, Landleven 12, 9747 AD Groningen, the Netherlands*
[e] *Department of Electronics and Nanotechnology, School of Electrical Engineering, Aalto University, Maarintie 8, 02150 Espoo, Finland*
[f] *Institute of Geophysics and Extraterrestrial Physics, Technische Universität Braunschweig, Mendelssohnstr. 3, 38106 Braunschweig, Germany*
[g] *Institute of Theoretical and Computational Physics, Graz University of Technology, 8010 Graz, Austria*
[h] *University of South-Eastern Norway, Raveien 215, 3184 Borre, Norway*
[i] *Institute of Geodesy and Geoinformatics, Wrocław University of Environmental and Life Sciences, Grunwaldzka 53, 50-375 Wrocław, Poland*
[j] *Laboratoire de Physique et Chimie de l'Environnement et de l'Espace (LPC2E), CNRS, Université d'Orléans, Orléans, France*
[k] *LESIA, Observatoire de Paris, PSL Research University, CNRS, Sorbonne Université, UPMC, Université Paris Diderot, Sorbonne Paris Cité, Meudon, France*
[l] *Politecnico di Torino, Corso Duca degli Abruzzi, 24, 10129 Torino, Italy*
[m] *Institute of Optical Sensor Systems, Deutsches Zentrum für Luft- und Raumfahrt e.V., Rutherfordstr. 2, 12489 Berlin, Germany*
[n] *Department of Systems and Space Engineering, Luleå University of Technology, SE-971 87 Luleå, Sweden*
[o] *Department of Physics, Umeå University, SE-901 87 Umeå, Sweden*
[p] *DEMec, Faculty of Engineering, University of Porto, R. Dr. Roberto Frias 400, 4200-465 Porto, Portugal*
[q] *Facultat de Física i Química, Universitat de Barcelona, Carrer de Martí i Franquès, 1, 11, 08028 Barcelona, Spain*
[r] *Space Research Institute, Austrian Academy of Sciences, Schmiedlstrasse 6, 8042 Graz, Austria*
[s] *Institute of Physics, University of Graz, Universitätsplatz 5, 8010 Graz, Austria*
[t] *Department of Physics, University of Oslo, Problemveien 7, 0315 Oslo, Norway*
[u] *German Aerospace Center (DLR), Institute of Space Systems, Robert-Hooke-Str. 7, 28359 Bremen, Germany*

Received 20 March 2023; received in revised form 10 November 2023; accepted 22 November 2023
Available online 25 November 2023

Abstract

Mars, lacking an intrinsic dynamo, is an ideal laboratory to comparatively study induced magnetospheres, which can be found in other terrestrial bodies as well as comets. Additionally, Mars is of particular interest to further exploration due to its loss of habitability by atmospheric escape and possible future human exploration. In this context, we propose the *Mars Magnetospheric Multipoint Measurement Mission* (M^5), a multi-spacecraft mission to study the dynamics and energy transport of the Martian induced magnetosphere comprehensively. Particular focus is dedicated to the largely unexplored magnetotail region, where signatures of magnetic recon-

* Corresponding author at: Zentrum für Astronomie der Universität Heidelberg, Astronomisches Rechen-Institut, Mönchhofstr. 12-14, 69120 Heidelberg, Germany.
E-mail address: cormac.larkin@uni-heidelberg.de (C.J.K. Larkin).

https://doi.org/10.1016/j.asr.2023.11.032
0273-1177/

nection have been found. Furthermore, a reliable knowledge of the upstream solar wind conditions is needed to study the dynamics of the Martian magnetosphere, especially the different dayside boundary regions but also for energy transport phenomena like the current system and plasma waves. This will aid the study of atmospheric escape processes of planets with induced magnetospheres. In order to resolve the three-dimensional structures varying both in time and space, multi-point measurements are required. Thus, M^5 is a five spacecraft mission, with one solar wind monitor orbiting Mars in a circular orbit at 5 Martian radii, and four smaller spacecraft in a tetrahedral configuration orbiting Mars in an elliptical orbit, spanning the far magnetotail up to 6 Mars radii with a periapsis just outside the Martian magnetosphere of 1.8 Mars radii. We not only present a detailed assessment of the scientific need for such a mission but also show the resulting mission and spacecraft design taking into account all aspects of the mission requirements and constraints such as mass, power, and link budgets. Additionally, different aspects of the mission programmatics like a possible mission timeline, cost estimates, or public outreach are shown. The common requirements for acceptance for an ESA mission are considered. The mission outlined in this paper was developed during the Alpbach Summer School 2022 on the topic of "Comparative Plasma Physics in the Universe".

Keywords: Mars; Induced magnetospheres; Multi-spacecraft constellation; Atmospheric escape; Mission concept proposal; Magnetic reconnection

1. Introduction

Among the planets in the solar system, Earth, Mercury, and the gas giants possess a global intrinsic magnetic field due to an active internal dynamo process. This is the dominant driver in the deflection and thermalization of the solar wind plasma. The region where the solar wind dynamic is influenced by the planet's magnetic field is called the magnetosphere. However, other planets such as Mars (Dubinin and Fraenz, 2015) and large solar system bodies like the Moon do not show such a dynamo and therefore lack a global intrinsic magnetic field. These bodies can still have local intrinsic magnetic fields — Mars possesses strong magnetic anomalies (crustal fields) of up to 700 nT at 200 km altitude, which are at least one order of magnitude more intense than the crustal fields on Earth (Langlais et al., 2019) — but in general, the large scale interaction with the solar wind of such systems is much different. For Mars, the direct interaction with the upper atmosphere generates the so called induced magnetosphere (Sánchez-Cano et al., 2021). The different regions of the Martian magnetosphere are presented in Fig. 1. Referring to the numbers in the figure, the Interplanetary Magnetic Field (IMF, 2) draped around the planet interacts with the solar wind (1), forming a bow shock (BS, 3) and a magnetic pileup boundary (MPB, 4), resembling the magnetopause at Earth, as dayside boundary regions (Trotignon et al., 2006) above the ionosphere (5). On the nightside, there is the magnetotail with its two lobes (7) that are separated by a plasma sheet (8), directed in opposite directions (Eastwood et al., 2008). Due to the induced character of the magnetosphere, the average sub-solar bow shock distance (3) at 0.63 planetary radii from the surface (Trotignon et al., 2006) is much shorter than compared to e. g. Earth at about 13 Earth radii. The crustal fields (6) of Mars can stand off the solar wind (Brain et al., 2003).

It is believed that Mars used to be more Earth-like, with a wetter and warmer climate. For this to have been the case, the atmosphere must have been denser than at present (Jakosky et al., 2017). Today, this is no longer the case, and in order to answer the question of how Mars became less habitable, we must investigate how the atmosphere was lost over time. This investigation starts with studying atmospheric loss in the present, from which one can then attempt to extrapolate the loss rates back in time. The absence of a global magnetic field makes the process different to that at Earth, specifically in terms of ion loss. Whether the presence of a global magnetic field protects the atmosphere from ion loss is up for debate, with some evidence suggesting that it actually increases ion escape (Gunell et al., 2018; Sakata et al., 2020; Ramstad and Barabash, 2021). The presence of crustal fields at Mars and the ensuing hybrid nature of its magnetosphere adds further complexity, with the crustal fields both inhibiting and enabling ion loss (Brain et al., 2010; Ma et al., 2014; Fang et al., 2017; Dubinin et al., 2020). Today, ion loss is a small part of the atmospheric loss at Mars, but may have been more significant in the past (Jakosky et al., 2018). Ions escape through a multitude of processes, many of which have been mapped by the MAVEN mission (Jakosky et al., 2018, and references therein). What is missing currently is consistent solar wind monitoring combined with simultaneous in situ measurements of the Martian magnetosphere, to enable studies of how these processes are affected by different solar wind conditions and by solar activity. By gaining a deeper understanding of ion loss dependence on different solar wind conditions and solar activity, further extrapolations can be made on how atmospheric escape has changed through time.

Additionally, the knowledge of space weather at Mars is an important driver for future exploration of Mars. Solar events, like interplanetary coronal mass ejections, Solar Energetic Particles, fast stream, etc., cause a high variability in the Martian magnetosphere (Hanaoka et al., 2023). This poses a threat to spacecraft and space infrastructure flying within the induced magnetosphere (Hassler et al., 2018), with possible catastrophic consequences (Marusek, 2007). Moreover, astronaut safety in the future manned exploration of Mars could be jeopardized if the conditions at Mars are not known in detail (Cucinotta et al., 2013).

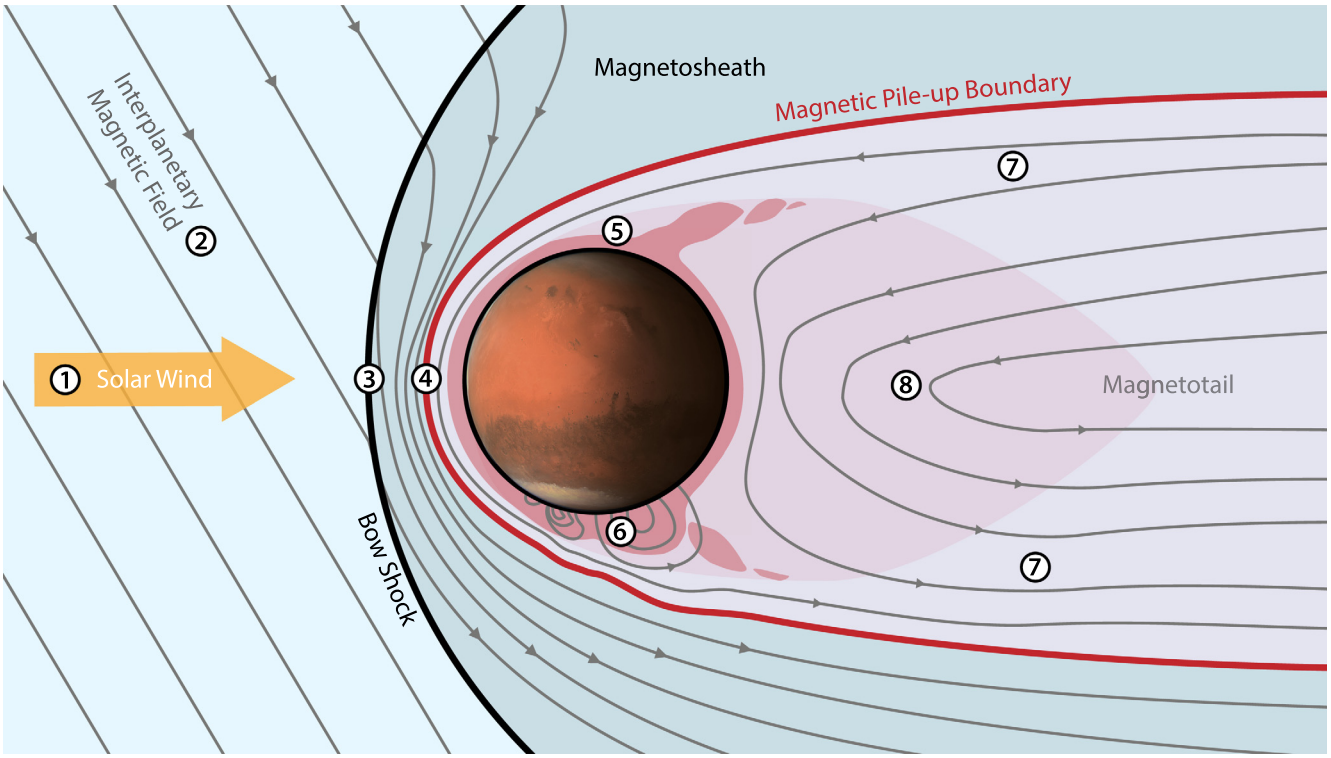

Fig. 1. Overview of the Martian induced magnetosphere. The Interplanetary Magnetic Field (IMF) is draped around the planet, forming boundary regions and a highly dynamical magnetotail that is yet to be studied in detail. The numbers indicate the different plasma zones addressed in the text. 1. Solar wind, 2. IMF, 3. Sub-solar point of the bow shock, 4. Sub-solar point of the magnetic pile-up boundary, 5. Ionosphere, 6. Crustal field, 7. Lobes of the magnetotail, 8. Plasma sheet of the magnetotail.

Therefore, near-continuous observations of the solar wind conditions at Mars are needed in order to both determine the average and extreme space weather conditions and determine their influence on the Martian magnetospheric system. Furthermore, a dedicated Martian solar wind observatory not only extends the "orchestra" of solar wind monitors, but also could aid in the study of the evolution of solar events.

Mars offers the opportunity to study an induced magnetosphere in greater detail. Due to Mars' proximity to Earth within the solar system, it can feasibly be reached by in situ instrumentation. Not only is it a representative example of a solar system induced magnetosphere (like Venus), but also relevant to studies of comets and active asteroids (Götz et al., 2019). Furthermore, if unique characteristic properties of such magnetospheric systems are identified, these could have implications for the characterization of exoplanetary plasma environments (Airapetian et al., 2020).

Changes in the IMF components induce a reorientation of the tail (DiBraccio et al., 2017), which is characteristic of this variability. In order to separate temporal and spatial variations of these moving or flapping structures in the tail, simultaneous multi-point measurements are needed. Despite comprehensive studies of the Martian environment of previous missions, the far tail region has never been characterized in detail by in situ measurements. A current open question is whether magnetic reconnection of the IMF occurs in the far tail at Mars, and if so, to what extent.

Magnetic reconnection is a fundamental plasma process where magnetic energy is converted to kinetic energy. It has been studied at Earth with formation missions like Cluster and the Magnetospheric Multiscale (MMS) mission. Similar processes occur on other magnetized and unmagnetized planets. On Mars, both measurements (Harada et al., 2015; Wang et al., 2021), and simulations (Ma et al., 2018) suggest that reconnection occurs on the nightside, playing a role in the dynamics of the magnetotail influencing ion flow velocities with possible effects on atmospheric escape.

Reconnection is not the only physical process of interest that takes place in the magnetotail. The magnetotail is one of the main paths for planetary ions to escape from the Martian atmosphere (DiBraccio et al., 2015; Brain et al., 2015; Dong et al., 2015; Dubinin et al., 2017; Lin et al., 2021; Curry et al., 2022). Therefore, a mapping of the properties of the Martian magnetotail complements ongoing studies of this important process and will allow a more complete assessment of balancing terms of atmosphere system in- and outflow. This is crucial for the understanding of how habitability of Mars has changed over time.

Moving from the Martian nightside to the dayside, important features of the induced magnetosphere are the BS and MPB. MAVEN (e.g. Jakosky et al., 2015) has

observed this region, showing a strong variation of the position of both BS and MPB (Matsunaga et al., 2017). However, a systematic characterization of their variability depending on solar wind conditions is lacking. Knowledge of the dependency of the system's short-term evolution on solar wind conditions — especially for solar high-energy events — is imperative for spacecraft and astronaut safety.

Energy transfer and transport, especially on global and ion-scales, is another important aspect of the characterization of the Martian magnetospheric system, which will help in understanding the complete picture of the evolution of the atmosphere. One of the ways to transport energy is by currents. A year-average picture of the Martian current system has been acquired by MAVEN (Ramstad et al., 2020), but a detailed, time-varying characterization is lacking. To measure the instantaneous current, a tetrahedral multi-spacecraft configuration is needed, in which methods such as the curlometer technique can be used, as it has been done at Earth for Cluster (Dunlop et al., 2021). This would allow the measuring of transient currents, which are lost in the process of averaging. Furthermore, by having a solar wind monitor, the response of the currents to changing solar wind conditions can be investigated.

Another way of transferring energy is through plasma waves, which are important to study due to their ability to accelerate and scatter particles, which can lead to the escape of particles from the atmosphere. Many waves around Mars have been identified, such as Whistler waves, Proton Cyclotron waves and Magnetosonic waves (Yadav, 2021; Brain et al., 2002). Other waves such as Ion Acoustic waves and Lower Hybrid waves are predicted to exist in the Mars ionosphere, but have yet to be detected (Yadav, 2021). The detection of the latter could explain some of the loss of particles from Mars outer ionosphere through particle acceleration. In order to fully characterize these waves, temporal and spatial variations would need to be resolved and separated, which requires a tetrahedron formation of spacecraft (Karlsson et al., 2004; Narita et al., 2010).

In order to allow for the separation of spatial and temporal variations of 3D plasma structures, again a four-spacecraft tetrahedron constellation is needed. This has been demonstrated by the Cluster mission at Earth (Escoubet et al., 2021). This mission allows the characterization of the time variation of the dayside boundaries and simultaneously determine their 3D spatial extent. Additionally, currents on above-ion-scales were detected by Cluster using the curlometer technique (Dunlop et al., 2021), as well as waves and turbulence with the wave-telescope technique (Narita et al., 2022) which are techniques only possible using four-point measurements.

Other missions at Earth have demonstrated how many important results can be obtained with a multi-spacecraft mission for space weather studies. The THEMIS mission, launched in 2007 and including five satellites, is designed to study space weather phenomena (Angelopoulos, 2009; Sibeck and Angelopoulos, 2008; McFadden et al., 2009). THEMIS also allows for the important study of Earth's boundary regions, characterizing the current sheet thickness, motion and current density of the magnetopause (e. g. Haaland et al., 2019), amongst many other important results (Přech et al., 2008; Li et al., 2009; Artemyev et al., 2020 and more). Another successful multi-spacecraft mission is MMS, a four-spacecraft plasma research mission dedicated to characterizing reconnection (Burch et al., 2016). MMS was the first spacecraft able to measure reconnection on electron scales, which was then studied by Burch and Phan (2016);Hesse et al. (2016); Shay et al. (2016) and many more. All this shows the success and need for a four-spacecraft constellation to study a planetary magnetospheric system comprehensively.

In the last decades, multiple missions have targeted Mars, tackling diverse science topics like the search for water and bio-signatures and the exploration of Mars' surface. The ongoing missions Mars Express (Chicarro et al., 2004) and MAVEN (Jakosky et al., 2015) have greatly contributed to our understanding of the Martian atmospheric composition, evolution and circulation. They are also equipped with plasma instrument suites, however are limited as for example Mars Express lacks a magnetometer. Additionally, the scientific output on the Martian magnetosphere is limited due to the lack of additional orbiters which would allow the observation of temporal and spatial variations. Moreover, there is currently no dedicated solar wind monitor at Mars, which is needed to investigate the variability of the magnetosphere depending on solar wind conditions.

The upcoming mission *Escape and Plasma Acceleration and Dynamics Explorers* (EscaPADE) — scheduled to launch in August 2024, arrive at Mars in September 2025, and officially start its science campaign March 2026 — will study the flow of both energy and ions in and out of the Martian atmosphere (Lillis et al., 2022). It will be the first twin-spacecraft space plasma mission beyond Earth's orbit. EscaPADE will have two consecutive science campaigns, the first a six month string-of-pearls configuration, and the second being separate orbits where the planes precess differentially. Its capacity to produce dual-point measurements will enable great scientific progress on the Martian plasma environment, upon which a multi-point mission could build. For instance, a tetrahedron configuration would uniquely enable the three-dimensional study of phenomena such as currents, waves and reconnection using known multi-spacecraft analysis techniques. By combining this with a solar wind monitor, the impact on these from varying solar wind conditions and solar activity could be studied. *Mars Magnetosphere ATmosphere Ionosphere and Surface SciencE* (M-MATISSE) is a mission currently being studied for the ESA M7 call aiming to characterise the region between the Martian upper atmosphere and the outer magnetosphere, and to study how surface processes are affected by space weather (Sanchez-Cano et al., 2022). Further upcoming missions to Mars include the Japanese Mars Moons Explorer (MMX) (Kuramoto

et al., 2022) mission which will be able to make magnetic field and suprathermal ion measurements including the solar wind, and the Tianwen-1 (Zou et al., 2021) mission which will have the capacity to measure the magnetic field and ions. Notably, DC electric field measurements were proposed as part of the MOSAIC 10-spacecraft constellation to study the Martian climate system from subsurface ice all the way to the solar wind (Lillis et al., 2021). However, none of the plasma missions sent to Mars to date have been capable of measuring DC electric fields.

Despite the considerable number of Martian exploration missions, there has been a paucity of plasma physics-focused missions in the past. Furthermore, both of the future dedicated plasma missions lack the capabilities to produce a complete and detailed picture of the structures and energy transport with both temporal and spatial dependencies in the whole Martian induced magnetospheric system as well as providing this information with dependency on precise upstream solar wind conditions.

All in all, the change of the magnetosphere with solar wind conditions and how energy is transferred across different scales — both spatially and temporally — remain to be fully understood. Additionally, the Martian magnetotail is still largely unexplored. This is reflected in the *Voyage 2050 Senior Committee Report* (Voyage 2050 Senior Committee, 2021), which was written to identify key science areas for ESA's science program during the period 2035–2050. Relevant key areas are "Magnetospheric Systems" (3.1.1) and "Plasma Cross-scale Coupling" (3.1.2). They state that, *"important questions such as 'How is energy and matter transported in induced magnetospheres' still need to be answered by studying entire magnetospheres as complex systems*". In this context, we propose the *Mars Magnetospheric Multipoint Measurement Mission*, hereafter M^5, a 5-spacecraft mission to study the different regions of the Martian magnetosphere comprehensively, by using a four-spacecraft tetrahedron formation for in situ measurements while monitoring the solar wind with an additional spacecraft.

This paper is organized as follows: in Section 2, the Scientific Objectives and Questions, derived from the above shown open research areas are given. With that, measurement requirements for different physical quantities to be measured at Mars are specified. Subsequently, the mission profile is described in Section 3, with the required scientific payload following in Section 4. In Section 5, all technical aspects of the proposed mission are assessed in detail. Finally, programmatics are addressed in Section 6 followed by a general conclusion (Section 7).

2. Scientific questions and measurement requirements

In order to structure the different regions and physical phenomena and make them more approachable from an instrument point of view, we define a broad scientific theme for the M^5 mission:*"To understand how the variable solar wind conditions influence the dynamics and energy transport of the Martian induced magnetosphere."*

From that, two primary scientific questions are derived, which are then segmented into scientific objectives. This hierarchy is shown in Table 1, including reference to the regions of interest shown in Fig. 1.

The first primary scientific question (**Q1**) focuses on the dependency of the Martian magnetosphere on solar wind conditions. The second question (**Q2**) relates to energy transport in the Martian magnetosphere. In addition to these two primary scientific questions, M^5 will be able to tackle two other secondary scientific questions. The third question (**Q3**) concentrates on the propagation of the solar wind in the solar system. The fourth question (**Q4**) is related to the possibility that reconnection in the Martian magnetotail is not the only process driving energy transport.

The respective scientific objectives allow for the definition of measurement requirements by using a traceability matrix. Table 2 shows the required measurement quantities for instruments on each spacecraft respectively, both on the *Solar Wind Observatory* (SWO) and the four *Magnetospheric Formation Orbiters* (MFO) constituting a tetrahedron constellation. The requirements were derived from each of the measurement regions, physical quantities, timing constraints, and specific measurement needs (e.g. range and accuracy) in question. The typical parameters that are expected to be observed by the M^5 missions are derived by previous in situ measurements (Nilsson et al., 2012; Holmberg et al., 2019; Ergun et al., 2021).

The requirements for magnetic field, ion distribution functions, electron distributions functions, and electric field measurements are detailed in Table 3, Table 4, Table 5, and Table 6 respectively. Based on the measurement requirements, corresponding heritage instruments or instrument options have been selected and are presented in Section 4.

3. Mission profile

To answer the science questions and objectives stated in Table 1, the M^5 mission requires a tetrahedral formation of four spacecraft. This allows the resolution of both spatial and temporal variations, as well as a three-dimensional mapping of the boundary regions, even when the location, velocity, and orientation of the boundary are unknown. This will result for example in the ability to take into account nonuniform conditions such as ripples and reformation, as has been done with Cluster. The same applies to the largely unexplored far magnetotail. In addition, such a constellation enables the mapping of currents in the magnetosphere, using the curlometer technique (Dunlop et al., 1988) to derive currents from magnetic field measurements. Furthermore, it will be used for measurements of wave direction and time dependency using the wave telescope technique (Motschmann et al., 1996). Finally, multiple spacecraft are needed to determine origin regions of magnetic reconnection by observing ion outflow. Spacecraft

Table 1
Scientific questions and objectives of the M[5] mission. The specific regions, that are referred to by the scientific objectives are given by numbers in parenthesis, corresponding to the regions specified in Fig. 1.

Primary scientific question	**Primary scientific objectives**
Q1: How do the Martian magnetospheric system's structure and dynamics depend on solar wind conditions?	O1.1 (1, 3, 4): What are the dynamics and orientation of boundary regions, with particular interest for their dependence upon solar wind conditions? O1.2 (1, 7, 8): What is the structure of the Martian magnetotail on different scales, with particular interest for its dependence upon solar wind conditions? O1.3 (1, 3, 4, 5, 7, 8): What is the dynamical structure of the current system in the Martian magnetosphere, with particular interest for its dependence upon solar wind conditions?
Q2: How is energy transported within the Martian magnetospheric system on ion scales and above?	O2.1 (7, 8): Is magnetic reconnection observed in the magnetosphere tail, and if so, where and how? O2.2 (3, 4): What are the direction and temporal evolution of low frequency plasma waves?
Secondary scientific question	**Secondary scientific objectives**
Q3: How does the solar wind propagate through the solar system?	O3.1 (1): What are the temporal variations of the upstream solar wind conditions at Mars?
Q4: Excluding magnetic reconnection, are there other processes driving the energy transport at the Martian magnetotail?	O4.1 (7, 8): Are other energy transport processes observed at the Martian magnetotail that exhibit signatures different to magnetic reconnection?

Table 2
Scientific objective addressed by each instrument used by the M[5] mission. A big dot ◯ stands for the Solar Wind Orbiter (SWO) and a small dot • for an Magnetospheric Formation Orbiter (MFO).

Science question	Science objective	DC vector magnetic field	Ion distribution function	Electron distribution function	Density, Temperature	DC vector electric field
	Magnetometer	Ion spectrometer	Electron spectrometer	Langmuir probe	Dipolar antennas	
Q1	O1.1	◯ • • • •	◯ •			
	O1.2	◯ • • • •	◯ •	◯	• • • •	
	O1.3	◯ • • • •	◯	◯		
Q2	O2.1	• •	• •			
	O2.2	• • • •			• • • •	• • • •
Q3	O3.1	◯	◯	◯		
Q4	O4.1	• •	• •	• •		• •

Table 3
Magnetic field measurement requirements

Requirement	In magnetosphere	In solar wind
Absolute range	3000 nT	500 nT
Absolute accuracy (per axis)	0.5 nT	0.5 nT
Temporal resolution	32 sps	32 sps

separation distances on and above ion scales are required to observe all the mentioned phenomena. Ion scales at Mars range from the proton gyroradius in the near tail on the magnitude of 100 km, to around 750 km maximum in the magnetosheath (Nilsson et al., 2012). In addition, an active solar wind monitor is needed to provide necessary simultaneous information about the solar wind conditions.

Therefore, we propose a five spacecraft mission. Four identical MFOs will be placed in an elliptic orbit in a tetrahedral cartwheel helix formation. The orbit is chosen in such a way that throughout a whole Martian year, the spacecraft spend a significant time in the far magnetotail. In its initial configuration, the dayside periapsis of the orbit is chosen just slightly larger than the expected bow shock stand-off distance, while the apoapsis is in the far magnetotail. This guarantees a sufficient number of boundary crossings. Orbit precession will gradually bring the apoapsis towards the dayside, thus allowing for a scanning of different boundary locations as well as the near tail region, as the periapsis moves to the nightside. A schematic of the orbits and the precession effects is shown in Fig. 2. Combined with a substantial orbit inclination, this way the MFOs will cover large portions of the Martian magnetotail and the boundary regions as well as the magnetosheath, addressing all primary science objectives of the mission. On-board fuel will allow for adjusting the tetrahedral configuration throughout the mission duration. Details of the final orbit configuration are given in Section 5.4.

Table 4
Ion moments measurement requirements

Requirement	In magnetosphere	In solar wind
Energy range	1 eV–30 keV	10 eV–25 keV
Energy resolution	25%	25%
Differential energy flux range	10^4–10^{10} eV/(eV cm^2 s sr)	10^4–10^{10} eV/(eV cm^2 s sr)
Temporal resolution	5 s	5 s
FoV	360°× 90°	180°× 40°
Ions to detect	H+, He++, higher mass	H+, He++, higher mass

Table 5
Electron moments measurement requirements

Requirement	In magnetosphere	In solar wind
Energy range	50 eV–10 keV	10 eV–5 keV
Energy resolution	25%	25%
Differential energy flux range	10^4–10^{10} eV/(eV cm^2 s sr)	10^4–10^{10} eV/(eV cm^2 s sr)
Temporal resolution	5 s	5 s
FoV	360°× 120°	180°× 40°

Table 6
Electric field measurement requirements

Requirement	In magnetosphere	In solar wind
Absolute range	±300 mV/m	–
Accuracy	1 mV/m or 10%	–
Temporal resolution	1 Hz–200 Hz	–

The fifth spacecraft, the *Solar Wind Observatory* (SWO), targets a circular orbit around Mars (see Fig. 2). The SWO will characterize the solar wind properties around Mars during the whole Martian year, thus addressing the secondary science question Q3, which supports addressing the primary science question Q1. As a result of the chosen orbit the SWO will spend a part of its orbit in the magnetotail, covering a region similar to the one explored by MAVEN. Furthermore, it acts as a data relay for the MFOs to Earth. Fig. 3 shows both the SWO and one MFO spacecraft in their final configuration at Mars.

4. Payloads

In this section, we provide an overview of the proposed instruments for the M^5 mission, in terms of the heritage instruments they are based on. The estimated resources required by the payloads are collected into Table 7 at the end of this section. Other, complementary instrumentation not considered here is discussed in Section 6.1.

4.1. Fluxgate magnetometer

The magnetometers proposed for the mission are 3-axis fluxgate magnetometers with heritage from THEMIS (Auster et al., 2008). Each spacecraft will carry a pair of these magnetometers mounted on different locations of a deployable boom stretching 4.5 m in length. One magnetometer will be located at the tip of the boom, whereas the other one halfway up the boom. This configuration allows for effective magnetic interference mitigation, as described in Section 5.6.9.

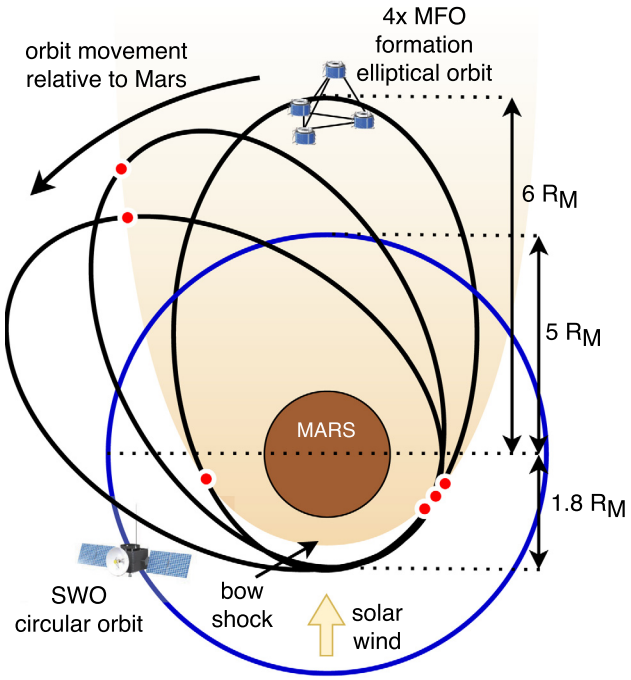

Fig. 2. Final orbit configuration of MFOs and SWO at Mars. Due to orbit precession, the orbit of the MFOs will move relative to the Martian reference frame during the Martian year "sweeping" over regions of interest (e.g. boundary crossings marked with red dots).

4.2. Ion spectrometers

The mission will utilize electrostatic analysers to measure the ion energy distribution function. The instrument placed on the SWO will be used as an ion energy spectrometer. A heritage instrument proposed for the task on the SWO is Solar Orbiter's SWA-HIS instrument (Owen et al., 2020).

In contrast, the instrument on each of the MFOs will use magnets to act as a mass over charge spectrometer. As heritage, the Ion Composition Analyser (ICA) instrument from Rosetta (Nilsson et al., 2007; Carr et al., 2007) is considered a viable option. The ion mass spectrometer will measure the 3D distribution function of the ions to study how the particles interact with the solar wind.

4.3. Electrostatic electron analyser

In order to measure the electron composition of the plasma environment, an electrostatic electron analyser will be employed on all five spacecraft. The heritage of the instruments is from the SWA-EAS instrument of the Solar Orbiter (Owen et al., 2020). The solar wind electron analyser will measure the effects from the electron impact ioniza-

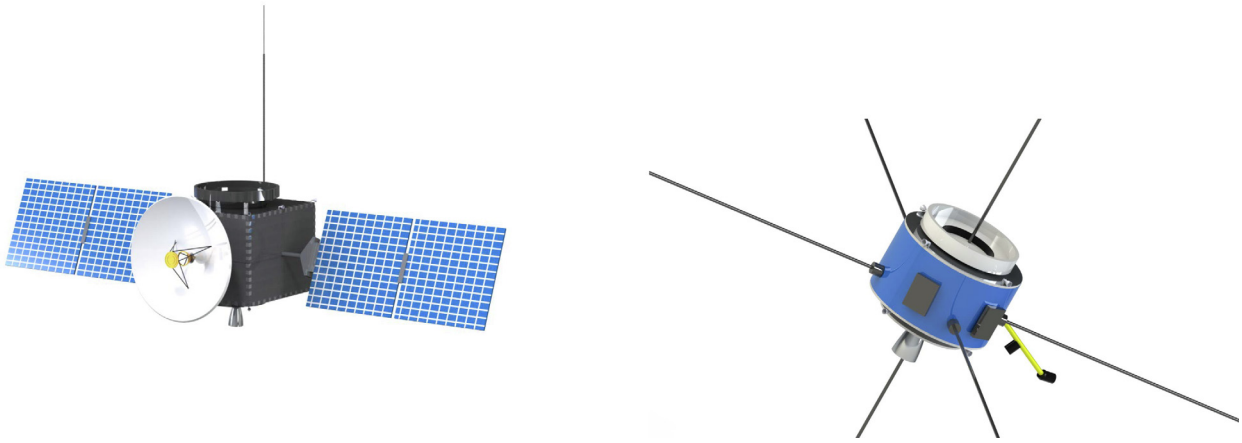

(a) The Solar Wind Observatory. (b) A Magnetospheric Formation Orbiter.

Fig. 3. Three-dimensional rendering of the two spacecraft types forming the M^5 mission.

Table 7
Estimated resources required by the payloads of the mission. Each resource estimate is given for a single payload. Power consumption refers to the nominal power consumption when the payload is in use. The estimates are based on the heritage instrument considered in Sections 4.1,4.2,4.3,.

Payload	Mass [kg]	Power [W]	Data rate [kbps]	References
Fluxgate magnetometer	0.4	0.8	6	a
Ion spectrometer (SWO)	2.2	2.8	6	b, c
Ion spectrometer (MFO)	2.2	2.8	1	c, d
Electrostatic electron analyzer	2.0	3.8	4	b
Electric field instrument (incl. booms)	14	3.7	1.5	e

[a] Auster et al. (2008)
[b] Owen et al. (2020)
[c] Carr et al. (2007)
[d] Nilsson et al. (2007)
[e] Gustafsson et al. (1997)

tion from the solar wind as it encounters the Martian atmosphere.

4.4. Electric field instrument

In order to measure the 3D electric field vector of the plasma environment, each MFO will have an electric field instrument using 6 booms (4 wire booms, 2 telescopic booms). In addition, two orthogonal probes will have Langmuir probe capabilities. This will be used to measure the temperature and density of the plasma. The instrument proposed for the described purpose is the electric-field and wave instrument (EFW) that has heritage from ESA's Cluster mission (Gustafsson et al., 1997).

5. Mission design

In the following, we will detail the technical aspects of the mission.

5.1. Margin philosophy

The margin philosophy adopted for the mission design is based on recommendations detailed by ESA (ESA, 2014). The applicable sections of the margin philosophy have been considered for all system budgets including mass, ΔV, propellant, data, and link budgets, as well as the power and thermal budgets.

5.2. Ground segment

For ground segment communications section, the ESA Deep Space Antennas network, which include the antennas located in Cebreros (Spain), Malargüe (Argentina) and New Norcia (Australia) will be used. Science operations will take place at the European Space Astronomy Centre (ESAC), close to Madrid.

5.3. Launch & propellant

The M^5 mission is designed to be launched using an Ariane 64 launcher from Kourou, French Guiana. Fig. 4 presents the M^5 mission spacecraft in the launch configuration inside the Ariane 64 fairing. After the launch, the five spacecraft will utilize thrusters with MMH/N204 bipropellant in order to perform the orbital and attitude maneuvers needed to reach and maintain the required orbits, stabilization, and attitude of the spacecraft. Helium pressurizing is used in order to maintain the operating pressures. Heritage thrusters from the ExoMars orbiter with a bi-propellant

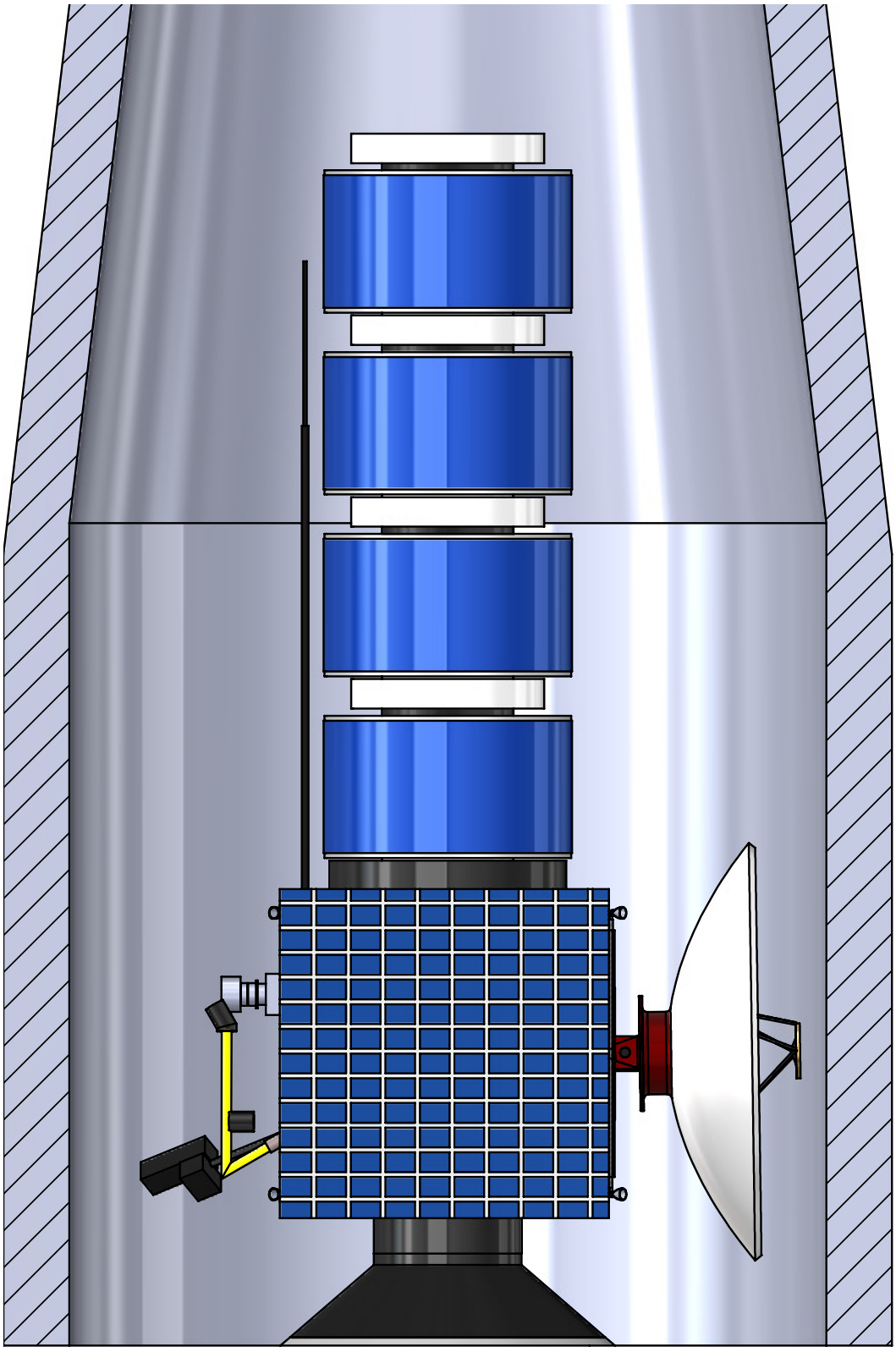

Fig. 4. Spacecraft in the launch configuration inside the Ariane's fairing.

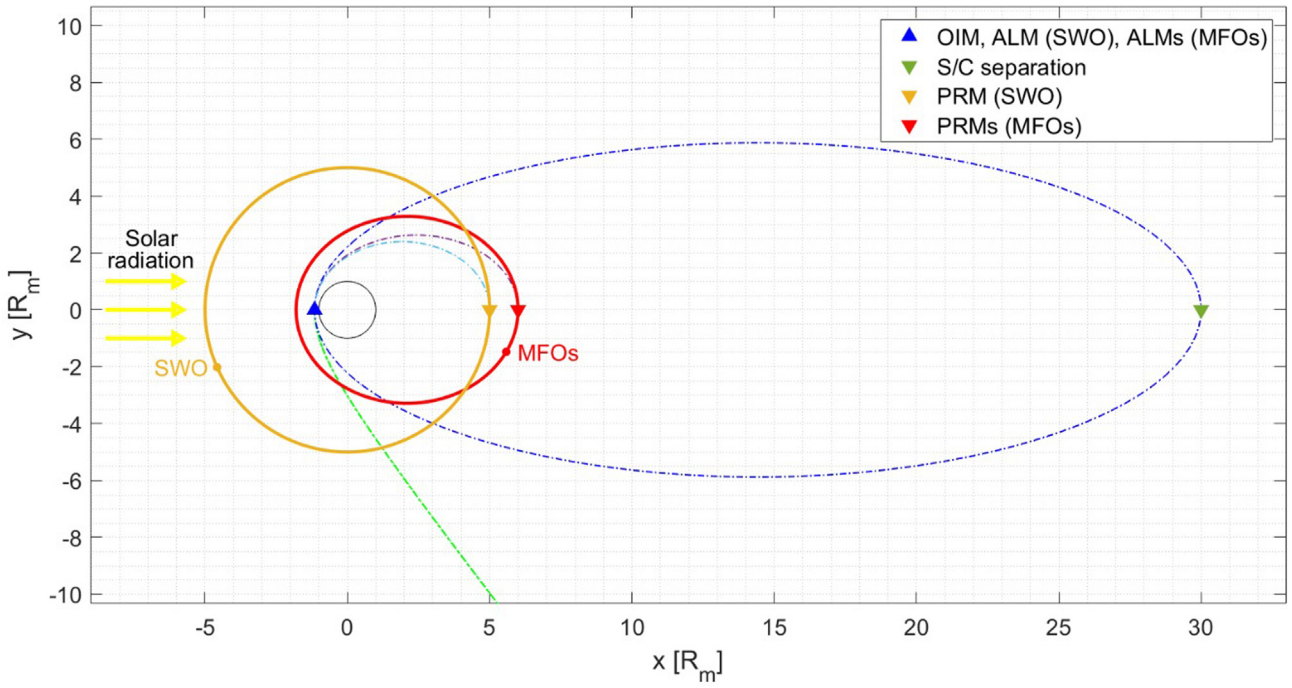

Fig. 5. Mission trajectory close to Mars in Mars-Solar-orbital coordinates. The approach trajectory of the five spacecraft is shown in green. At the end of the approach trajectory an Orbit Insertion Maneuver (OIM) is performed to reach the capture orbit show in blue. Following the OIM the spacecraft separate. From the capture orbit, SWO lowers first its apoapsis, and finally increases its periapsis to reach its circular target orbit ($5R_m \times 5R_m$) shown in orange. After the SWO has finished its maneuvers, the MFOs lower their apoapsis and raise their periapsis to reach their target orbit ($1.8R_m \times 6R_m$) shown in red. The inclination of the orbital plane is 150° for all orbits. A more detailed description of the maneuvers is provided in Section 5.4. (For interpretation of the references to colour in this figure legend, the reader is referred to the web version of this article.)

propulsion system (Pavón et al., 2012) are proposed for the M^5 mission.

5.4. Orbits & maneuvers

After launch, the five spacecraft will fly in a stacked configuration along a heliocentric elliptic transfer orbit to Mars. The approach trajectory along with the final orbits of the spacecraft and the transfer orbits needed to reach them are illustrated in Fig. 5. Initially the four MFOs are stacked on top of the SWO. In this transit configuration the spacecraft will perform a number of Trajectory Correction Maneuvers (TCMs) before reaching Mars' sphere of influence, arriving at a periapsis of $1.15R_m$ with an inclination of 150°. In the stacked configuration, the spacecraft perform an Orbit Insertion Maneuver (OIM) that brings them to a capture orbit with a periapsis of $1.15R_m$ and an apoapsis of $30R_m$. The low periapsis and high apoapsis of the capture orbit is chosen to maintain the propellant mass of the SWO within feasible limits set by the size of the SWO inside the launcher fairing.

Approaching the apoapsis of the capture orbit, approximately 48 h after the OIM, all five spacecraft separate mechanically from each other. The early separation of the spacecraft is, again, a trade-off between the limited SWO propellant mass and an increase in mission operations complexity that arises from individual maneuvering of the spacecraft. Once all spacecraft reach the periapsis following the separation, the SWO performs an Apoapsis Lowering Maneuver (ALM) to bring it to a $1.15R_m \times 5R_m$ orbit. As soon as the SWO reaches the apoapsis of this new orbit, it will further perform a Periapsis Raise Maneuver (PRM) to circularize its orbit to its target orbit ($5R_m \times 5R_m$). The MFOs, in contrast, continue an additional rotation along the capture orbit to avoid performing maneuvers simultaneously with the SWO. Once the MFOs reach the capture orbit periapsis again, they perform simultaneous ALMs to obtain a $1.15R_m \times 6R_m$ orbit. When the MFOs reach the apoapsis of this orbit, they perform PRMs to obtain their target orbit of $1.8R_m \times 6R_m$. Finally, the MFOs perform a Formation Configuration Maneuver (FCM) to reach the required cartwheel helix formation. The ΔV required to perform the required orbital maneuvers and the propellant mass burned during the thrusts are presented in chronological order in Table 8.

The choice of orbit for the MFOs ($1.8R_m \times 6R_m$) satisfies the scientific requirement of orbiting in the magnetotail. The 150° orbital inclination that all spacecraft maintain throughout the mission is chosen to maximize the benefit obtained from the J_2 effect. Due to the optimized utilization of the J_2 effect, the time spent in the tail region is increased by a factor of five to 280 days. A schematic of the orbit propagation can be seen in Fig. 2, and the simulated temporal evolution of the orbits is shown in Fig. 6.

Table 8
ΔV budget. The maneuvers are presented in chronological order. A symbol × indicates which spacecraft perform(s) the maneuver in question. Before spacecraft separation, the spacecraft are in a stacked configuration, and the SWO is responsible for the maneuvers. The spacecraft separation is performed mechanically and requires no propellant. The required ΔV and propellant mass is always indicated for a single spacecraft (or for the whole spacecraft stack prior to separation).

Maneuver	ΔV [m/s]	SWO	Each MFO	Propellant mass [kg]
TCMs	10.5	×		6.2
OIM	808.2	×		467.7
Spacecraft separation	–	×	×	–
ALM	392.3	×		65.7
PRM	648.4	×		114.6
ALM	321.51		×	22.7
PRM	170.9		×	11.2
FCM	420		×	25.1

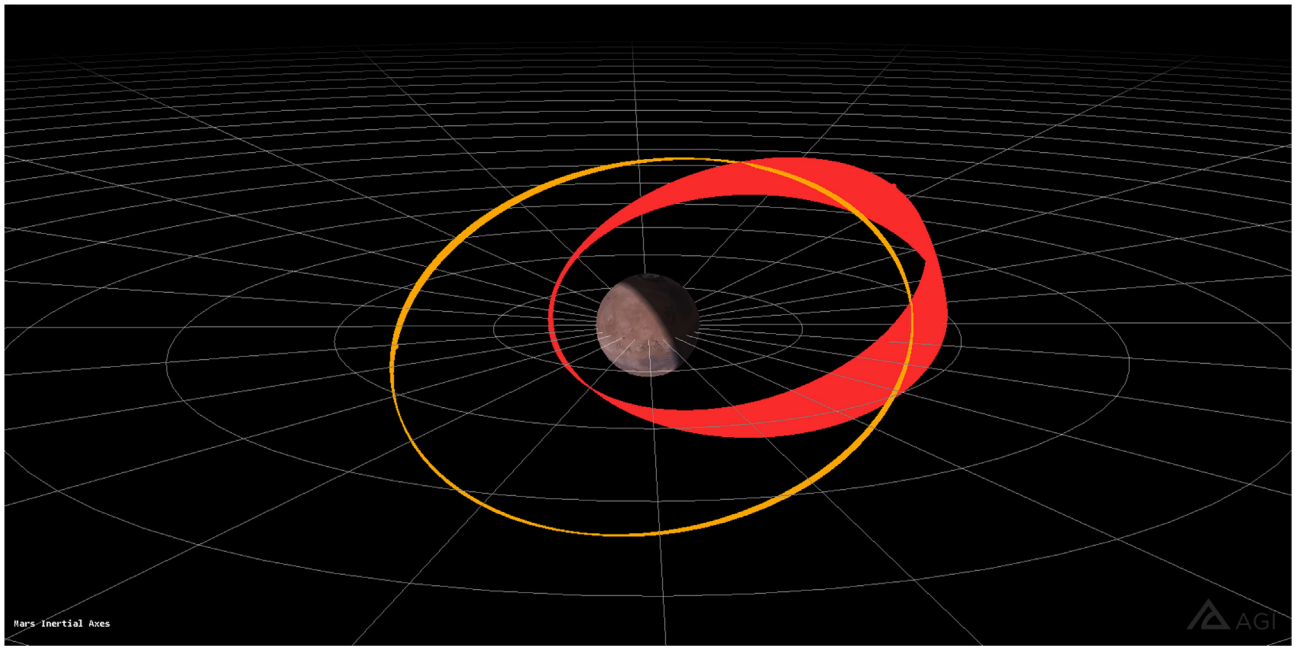

Fig. 6. Orbits propagated for 100 days. The orbit of the SWO is shown in orange, and the orbit of the MFOs in red. J_2 perturbations will move the RAAN of the MFOs' orbit over time at a constant rate of 0.22° per day. The figure is a screen capture from the STK simulation software.

5.5. Orbit & attitude maintenance

In addition to propellant required for the ΔV to reach the required Martian orbits, propellant is budgeted for orbit maintenance and attitude control over the mission lifetime. Orbit Trim Maneuvers (OTMs) are required to maintain and fine tune the orbits. The propellant mass required for OTMs of each spacecraft is estimated based on the experience gained from the MAVEN mission (Jesick et al., 2017). Attitude Control Maneuvers (ACMs) augment the use of reaction wheels to adjust or maintain the attitude of the spacecraft. ACMs include periodical thruster firings for offloading torques from the reaction wheels to keep them out of saturation. The propellant allocated for OTMs and ACMs is 21.1 kg for the SWO and 7.4 kg for each MFO. Attitude control details and requirements are presented in Section 5.6.8.

5.6. Space segment

The space segment of the mission consists of the SWO and the four MFOs, which differ in design due to varying payloads and functionalities. The following subsections cover the space segment in more detail.

5.6.1. Structure & spacecraft design

The primary structure of both types of spacecraft consists of a 1.214 m cylindrical core that encloses the propellant tanks, made of titanium (Ti6AI4V STA). Exterior panels are attached to the central core. An aluminium honeycomb sandwich structure with graphite composite face sheets is used for all the primary structure elements of both configurations, providing enough stiffness to sustain the launch loads and induced vibrations. The panels sections are joined with bonded composite L-brackets. The general dimensions of the SWO spacecraft are 2.3 m × 2.3 m

× 1.8 m, whereas the MFOs have a diameter of 1.5 m and a height of 1.2 m. The preliminary dry mass of the structure alone is estimated to be 240 kg for the SWO and 90 kg for each MFO. The material structure and structure layout employed is widely used in space missions (Yasaka and Onoda, 2003). This provides a high TRL, and heritage e.g. from the Dawn (Thomas et al., 2011) and MAVEN (Jakosky et al., 2015) spacecraft for the SWO and Cluster (Escoubet et al., 1997) for the MFOs.

In the bottom part of the spacecraft, a central cylinder is used to ensure precise attachment to the payload adaptor. On the top part of the spacecraft, an attachment and locking mechanism is used. The MFOs are stacked on top of each other using the aforementioned locking mechanism which will be designed in further mission design phases. An exploded view of the SWO with major subsystems is presented in Fig. 8.

5.6.2. Mass budget

To calculate the mission mass budget, the mass of each subsystem was derived based on estimates and data on existing subsystems. The estimated payload masses are presented in Table 7. A margin of 5% to 20% was added to the calculated mass of each subsystem. Moreover, an additional overall system margin of 20% was added to the sum of subsystem masses to obtain the final dry mass estimate of the system. The total wet mass of the system was obtained by adding up the dry mass and the required propellant mass with margins. The margin philosophy is explained in Section 5.1. The mass budget that shows the masses of each spacecraft and the total system mass is presented in Table 9.

Table 9
Final mass budget.

Spacecraft	SWO [kg]	1 MFO [kg]	Margin
Dry mass	517	182	–
Dry mass (marg.)	621	218	1.20
Propellant (marg.)	730	69	1.10
Total mass	1364	288	–
2516 kg	–	–	–

5.6.3. State modes

The SWO and MFO will operate in seven different main state modes presented in Fig. 7. The different state modes are designed for different phases of the mission. At the beginning of the mission, during launch and part of the transit, the system will stay in Safe Mode. This is a low power mode where as many subsystems as possible are turned off, and special safety measures are taken to ensure they will not turn on unexpectedly in any critical phase at the start of the mission. In addition, unintended separation of the spacecraft from each other should be strictly prevented.

From Safe Mode the system will proceed to Commissioning Mode, where e.g. solar panels are deployed in order to start power generation and health checks are performed on the instruments. Sun Safe Mode is entered after commissioning for the duration of the transit. It ensures that the system generates power, but payloads stay powered down or in a low power mode. Orbital Control Mode is entered as the spacecraft arrives at Mars. This mode enables orbital maneuvering utilizing the thrusters of the spacecraft. The mode is critical for reaching the desired orbits of the spacecraft, and performing small corrective maneuvers later on during the mission.

When the required orbits are reached, the spacecraft can proceed to start the science phase of the mission by operating in Science Mode. In this mode the spacecraft are designed to operate all of their instruments in order to collect data. At specific events during the mission, e.g. boundary crossings, the so-called Burst Mode can be initiated to enable short periods of increased data acquisition rates for the instruments. Science operations are not allowed in Safe Mode or during data transmission.

For transmitting the generated data, each spacecraft can enter Downlink Mode. For the MFOs this enables data transmission to the SWO. Furthermore, the SWO is able to downlink the self-generated data and the data received from the MFOs to the ground station on Earth. Receiving

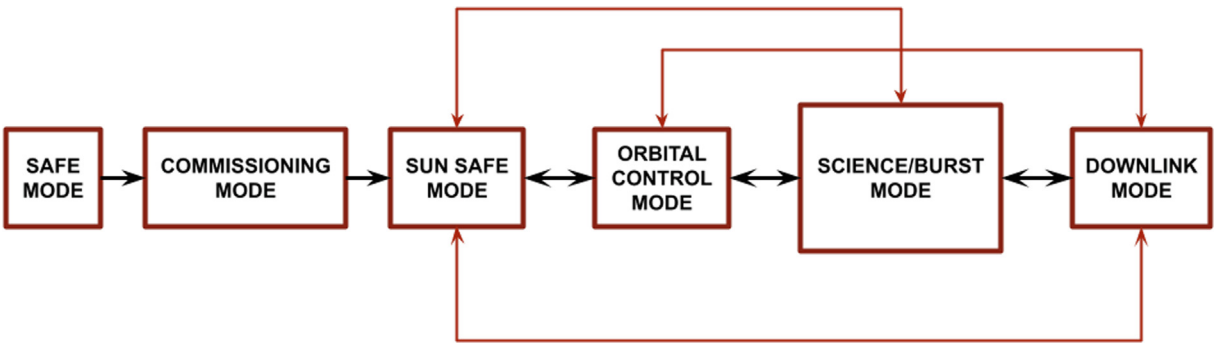

Fig. 7. State Mode Diagram. Arrows depict the possible transitions between different modes. In general, any state mode is accessible directly from any other state mode. The exceptions are Safe Mode and Commissioning Mode, which are not used after they have been completed at the early phases of the mission. Sun Safe Mode acts as the contingency mode after launch.

is activated in most state modes to enable commands to be sent to the spacecraft. The only exceptions are Safe Mode and Sun Safe Mode during transit, where only the SWO is receiving, as the spacecraft are still attached together.

In the following sections, Safe Mode and Sun Safe Mode can together be referred to as "safe modes", whereas "nominal modes" refer to all other operating modes.

5.6.4. Power budget

The power budgets of the spacecraft have been designed by assuming worst case solar irradiance conditions, as well as end-of-life conditions for different parts of the power system. This means that e.g. the degradation of solar cells and batteries over the mission lifetime has been accounted for when sizing the system. The estimated power consumption of each payload can be found in Table 7. The total power consumption of the SWO in nominal state modes at the Red Planet will range from a maximum of 440 W (Downlink Mode) to 240 W (other nominal modes). The power generated by the SWO's solar panels in the Sun will be 400 W at Mars. In contrast, the total power consumption of the MFO will vary between 250 W (Downlink Mode) and 150 W (other nominal modes). The power generated in the Sun by an MFO at Mars will be 250 W.

All nominal state modes of a spacecraft, except Downlink Mode, consume the same amount of power. This results from sufficient heat dissipation being the restricting factor that determines the lower limit for power consumption. The reason for the higher power consumption of Downlink Mode is that in addition to the heat required to maintain the thermal balance of the satellite, some power is also radiated away from the satellite in transmission. Furthermore, for the SWO, Downlink Mode is considered in two separate submodes: transmitting to Earth, or transmitting to the MFOs. When transmitting to the MFOs, the SWO can use its payloads without compromising the thermal or power budget.

In the safe modes, Safe Mode and Sun Safe Mode, the power consumption can potentially be lower than in nominal state modes. For example, during transit in Sun Safe Mode, the spacecraft are closer to the Sun than they are at Mars, and the required heating power produced by the spacecraft is lower. Additionally, if the power balance of a spacecraft would become compromised during nominal operations at Mars, the Sun Safe Mode can be initiated

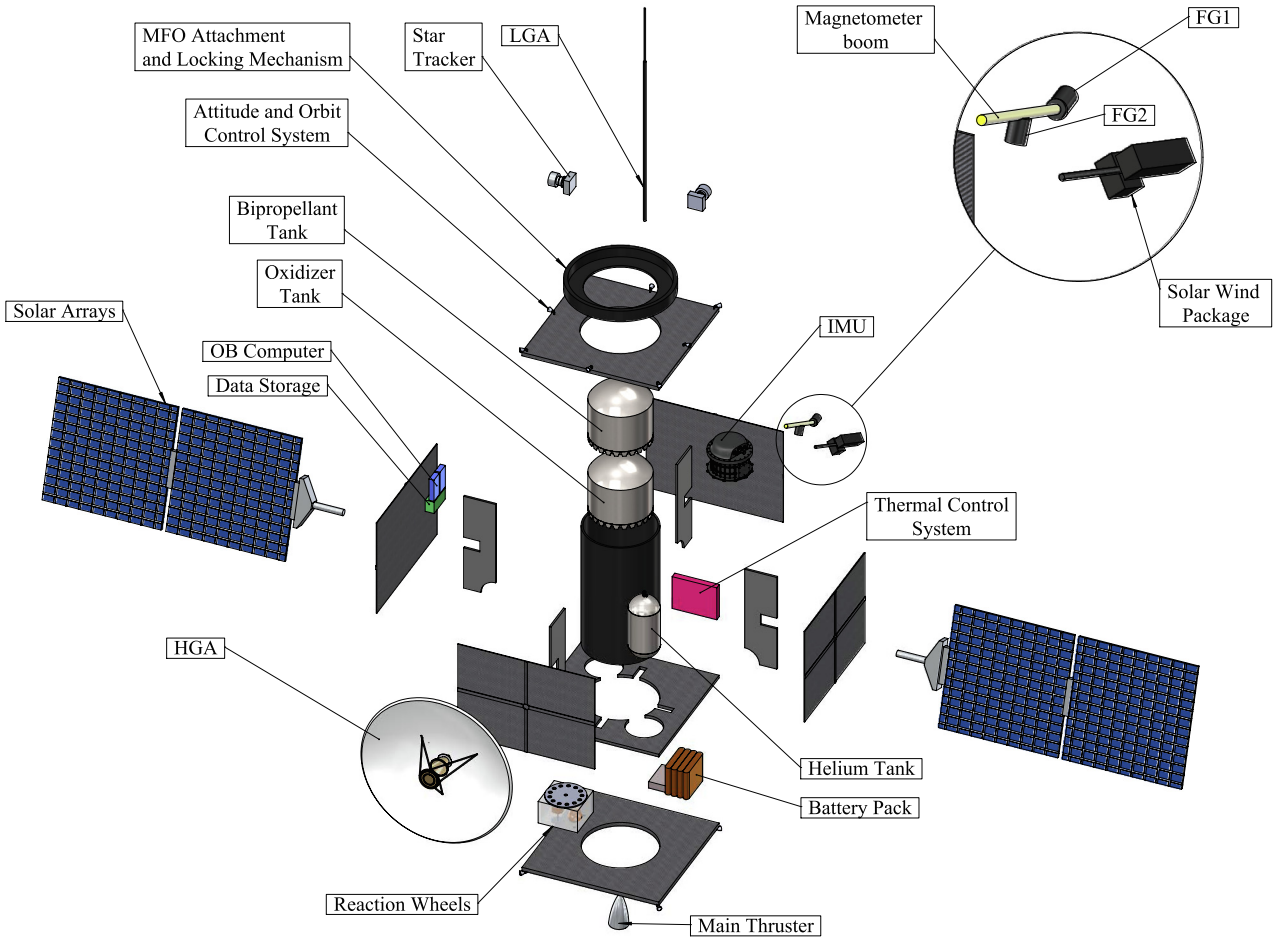

Fig. 8. Expanded view of the Solar Wind Observatory and all major subsystems. Some small-sized subsystems are scaled up for improved visualisation.

in order to save power while waiting for the batteries to recharge. The power consumption of different state modes is illustrated in Fig. 9.

In the safe modes, the main factor limiting how low the power consumption can be decreased is the requirement to maintain the thermal balance of the spacecraft on a level that does not harm the spacecraft or their subsystems. The required power can be minimized, if the most temperature sensitive components are placed close to each other, and they are thermally well isolated from the environment. However, the tentative thermal modelling of the spacecraft does not enable detailed estimations of the power consumption in the safe modes during different mission phases. The detailed analysis of the power consumption in the safe modes will be performed in later mission design phases.

The estimated maximum eclipse time during the mission is 71 min for the SWO, and 112 min for the MFOs. The designed solar array power generation capacity is sufficient to charge the batteries of both types of spacecraft between the eclipses while staying in nominal operation modes. Without accounting for Downlink Mode, power is produced with a margin of approximately 50% compared to the other nominal state modes. Accounting for the higher power consumption of Downlink Mode reduces the margin

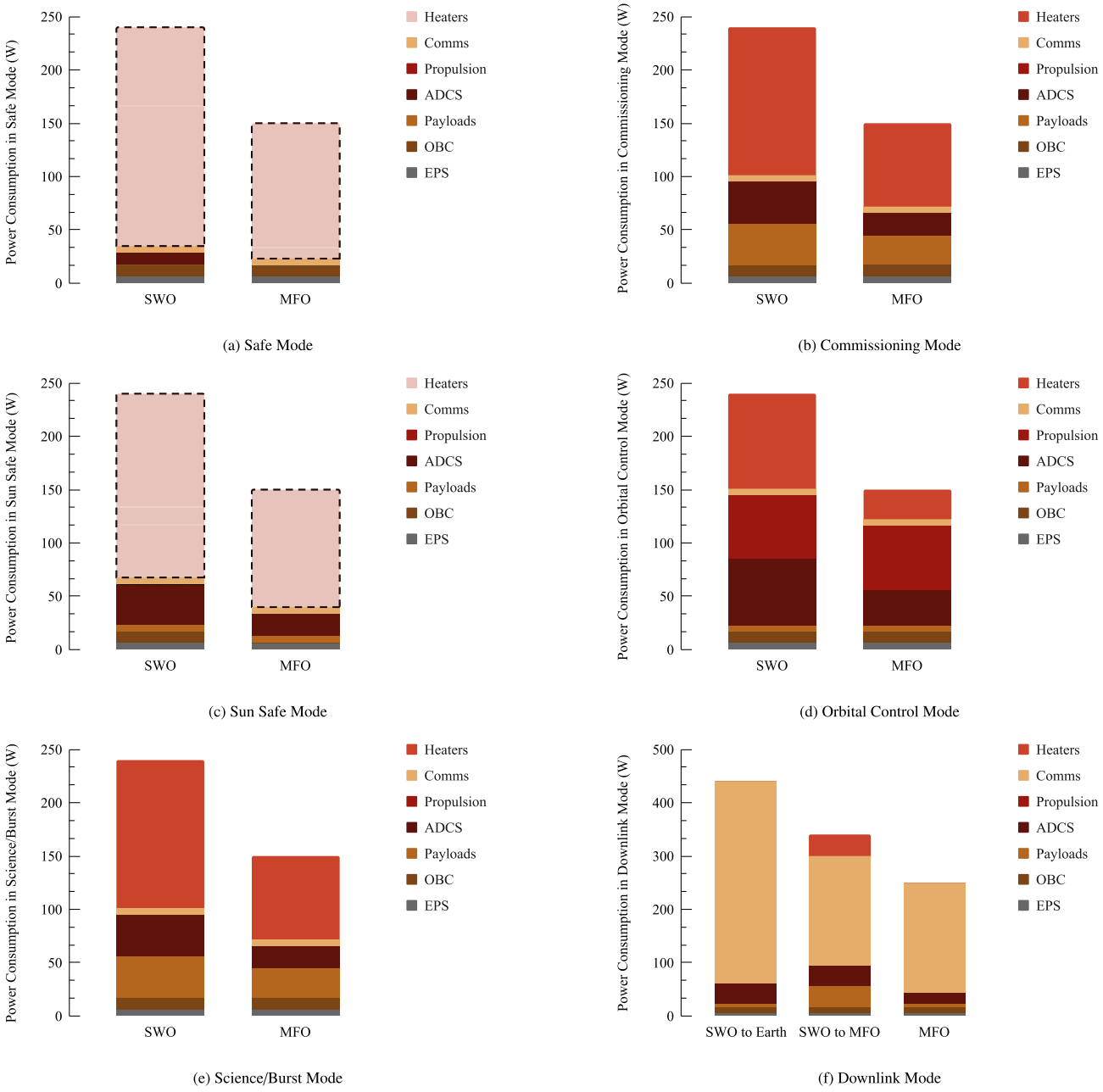

Fig. 9. Power consumption in different state modes of the SWO and an MFO. Note the different scale of the vertical axis for Downlink Mode. In addition, note that in Safe Mode and Sun Safe Mode, the total power consumption may be lower than the total shown in the figure. The uncertain part is illustrated with a lighter box surrounded by a dashed line. The power budget is presented in detail in Section 5.6.4.

significantly, but battery capacity is sized to enable the downlink sessions required during the mission (see Section 5.6.6). The batteries used for the SWO and each MFO are 3000 Wh and 1500 Wh silver-cadmium batteries respectively. If, for any reason, the power balance of any of the spacecraft would become compromised, the Sun Safe Mode can be initiated in order to save power while waiting for the batteries to recharge.

5.6.5. Thermal budget

For thermal modelling of the spacecraft, a coarse overall spacecraft thermal mathematical model (TMM) was utilized. The tentative modelling shows that to stay inside the estimated nominal operating temperature range with margins (−20 °C to 60 °C), the SWO and each MFO require a continuous average heat dissipation of 240 W and 150 W respectively. As subsystem heat dissipation alone does not reach the required level, heaters are used to generate the required total heat. In addition, multilayer insulation (MLI) is considered for thermal insulation of the spacecraft. No active cooling is required to maintain the spacecraft temperature according to this estimate, provided sufficient heat transfer within the spacecraft to even out internal thermal gradients. At later system design phases, a more sophisticated thermal control scheme could be devised to optimize the power consumption and thermal stability of the spacecraft. As of now, the feasibility of the thermal budget has been demonstrated by assuming simple constant thermal dissipation power.

As all power produced by the subsystems on-board the spacecraft (except power radiated from the antennas in Downlink Mode) is assumed to be dissipated as heat in the spacecraft, the total heat dissipation budgets are equal to the power budgets in each operating mode (except Downlink Mode). In Downlink Mode, the heat dissipation of the SWO is 200 W lower than the power consumption. Similarly, the heat dissipation of a MFO is 100 W lower than its power consumption in Downlink Mode.

5.6.6. Telemetry budget & telecommand

In addition to performing scientific measurements, the SWO serves as a communication relay between the MFO formation and the ground segment on Earth. For this purpose, the SWO carries a high gain dish antenna (HGA) with a diameter of 2.5 m. The X-band is chosen for the data link between Earth and Mars, similarly as has been done for instance on the Mars Reconnaissance Orbiter (Graf et al., 2005). The strict pointing requirement of the HGA (<0.3°) is achieved by pointing the antenna semi-independently from the spacecraft body. To enable communications between the SWO and the MFOs, each of the five spacecraft carries a low gain dipole antenna (LGA) that poses no strict pointing requirements. Communication between the MFOs and the SWO will use the S-band frequency range, which was shown by link calculations to be suitable for the intersatellite link.

The link budget of the mission is heavily dependent on the mutual distances between the spacecraft, as well as the distance of the SWO from Earth. The simulated best and worst case distances, as well as the average distance over time, are presented in Table 10. The corresponding link budgets are detailed in Table 11. The significant variance in downlink rates is attributed to differences in free-space path loss (FSPL) that depends on the distance between the transmitter and receiver. FSPL grows rapidly as distance d between the transmitter and the receiver increases (FSPL $\propto d^2$), and leads to signal attenuation.

A majority of the proposed scientific heritage instruments (see Section 4) enforce lossless compression on their measurement data or stream continuously low resolution data while storing high resolution data to be transmitted only on demand. The maximum estimated total data volume produced by the instruments is presented in Table 12. The result is based on the estimated data rates of each payload detailed in Table 7. The data rate estimations are designed to account for both nominal Science Mode operations and higher data rate Burst Mode measurements. A significant margin of 50 % has been added to the tentative

Table 10
Mutual distances during the mission. The mean distances are weighted by time.

	Min.	Max.	Mean
SWO/Earth	5.7×10^7 km	3.2×10^8 km	1.5×10^8 km
MFO/SWO	1.2×10^3 km	3.7×10^4 km	2.0×10^4 km

Table 11
Link budget as achievable downlink/uplink data rates that correspond to the distances specified in Table 10.

Direction	Min.	Max.	Mean
SWO → Earth	0.72 Mbps	24 Mbps	3.5 Mbps
Earth → SWO	2.1 Mbps	67 Mbps	9.9 Mbps
MFO → SWO	6.4 kbps	6.2 Mbps	22 kbps
SWO → MFO	6.4 kbps	6.2 Mbps	22 kbps

Table 12
Maximum combined instrument data rate averaged over an orbit.

Unit	Max. data rate	Duty cycle	Mean data rate
SWO	19 kbps	50%	9.4 kbps
MFO	23 kbps	65%	15 kbps
Total	112 kbps	–	70 kbps

Table 13
Downlink times for the amount of data produced over an average 24 h period.

Direction	Min.	Max.	Mean
SWO → Earth	6 min	3.4 h	42 min
MFO → SWO	4 min	57 h	17 h

estimations that are based on data rates specified for the proposed heritage instruments.

Table 13 shows estimated downlink times for the amount of data produced during an average 24 h period of mission operations. The downlink times are estimated between the different spacecraft, as well as between the SWO and the ground station network. The SWO achieves downlink times of 3.4 h even in the worst case scenario, corresponding to a total of 15% of operation time on average. This enables downlinking all data produced by the SWO and the MFOs to Earth with good margin during the whole mission duration, independent from the mutual distance of Earth and Mars.

The MFOs, in contrast, require optimized downlink schedules to be able to transmit all science data to the SWO, as the worst case and mean downlink rates are too slow for efficient data transfer, but the best case downlink rate is excellent. The downlink sessions should be scheduled to take place when the distance between the MFOs and the SWO is close to minimum to ensure the downlink time is minimized. As the orbital periods of the SWO and the MFOs are 18.6 h and 12.8 h respectively, the spacecraft will undergo a sufficiently close encounter roughly every 38 h. The amount of on-board data storage is sufficient to store the data produced over significantly longer periods of time than the time between adjacent downlink time slots (see section Section 5.6.7). Thus, not all downlink opportunities have to be utilized. Downlink opportunities can occasionally be skipped, e.g. if the opportunities happen to occur during particularly interesting measurement possibilities, such as magnetotail border crossings or exceptional solar wind conditions.

The uplink times from the SWO to the MFOs or from Earth to the SWO will be short, since the transmitted data volumes are minor, as only short commands need to be transmitted in these directions. In addition, the uplink data rate from Earth is relatively high during the whole mission lifetime.

5.6.7. On-board computer and data storage

The radiation hardened RAD-750 onboard computer (OBC) proposed for the mission has heritage from several missions such as the Mars Reconnaissance Orbiter (Graf et al., 2005) as well as the Curiosity (Welch et al., 2013) and Perseverance (Abcouwer et al., 2021) rovers. As the SWO poses a major single point failure risk for the mission, the spacecraft is equipped with two redundant OBCs. The four MFOs are each equipped with a single RAD-750 OBC.

The onboard data storage allocated for each MFO is 30 GB, whereas the SWO will carry 160 GB of memory. The combined total data storage is designed to be sufficient for storing the total data produced by all spacecraft over an average 12 month period. This is possible, as an MFO can store the data produced by itself over 6 months, whereas the SWO can store the data produced by each MFO over 6 months, as well as the data produced by itself over 12 months. The amount of data storage contains substantial margin to enable significant flexibility in downlink scheduling (see Section 5.6.6).

5.6.8. Attitude determination & control

For attitude determination, each spacecraft will use an inertial measurement unit (IMU) in combination with two star trackers. The star trackers are utilized for periodical IMU calibration, and they offer a redundant means of attitude determination. The SWO carries four reaction wheels for standard attitude and pointing control and a total of twelve thrusters: one main thruster for orbital insertions and major orbital maneuvers accompanied by eleven smaller thrusters for attitude control and minor orbital maneuvers. Each of the spin stabilized MFOs will also carry twelve thrusters in a similar configuration.

The high gain antenna of the SWO requires a pointing to Earth with $<0.3°$ error for downlink mode. The HGA can be pointed semi-independently from the rest of the SWO spacecraft body. The low gain dipole antennas of all the spacecraft are required to maintain an alignment with the normal of the orbital plane with $<30°$ of error in order to obtain a data link between the SWO and the MFOs.

During science mode operations, the solar wind observing instruments of the SWO require a pointing accuracy of $<10°$ towards the incoming solar wind. The MFOs are required to spin in orbit in order to extend their wire booms. The measurements do not impose any pointing requirements on the MFOs.

5.6.9. Electromagnetic interference considerations

As accurate and high resolution measurements of the Martian magnetosphere are key to the scientific goals of the mission, strict magnetic cleanliness of the spacecraft will be necessary to prevent unwanted interference from impacting measurements. A key measure taken to reduce the magnetic disturbances caused by the spacecraft is to "back wire" the solar panels. The back wiring method reduces solar panel current loops, and consequently the magnetic field disturbances induced by the loops. The method has successful heritage from missions such as Mars Global Surveyor (Acuna et al., 1996) and MAVEN (Jakosky et al., 2015).

To limit the influence of remaining spacecraft-induced magnetic fields on the measurements, all fluxgate magnetometers are placed on 4.5 m long booms. Additionally, each spacecraft has two magnetometers on the same boom to allow for cleaning of magnetic field data. The primary scientific magnetometer is placed on the tip of the boom, whereas the second one, closer to the spacecraft body, acts as an auxiliary magnetometer that assists in identifying and removing potential magnetic interference by the spacecraft from the data. This approach has previously been employed e.g. on the Cluster mission (Balogh et al., 1997).

Electromagnetic interference must be considered also from a communications perspective to ensure the space-

craft are not producing interference on their communication frequencies in the S- and X-bands.

5.7. End-of-life & planetary protection

ESA missions are required to abide by planetary protection standards. M^5 would be classed as a Category III mission by the relevant planetary protection standard (ECSS-U-ST-20C, 2019). Therefore, this mission will inventorise and retain samples of organic materials used in the spacecraft, comply with bioburden requirements, and assemble the spacecraft in a cleanroom of ISO class 8 or above. The mission is also required to have an impact probability $\leqslant 1 \times 10^{-4}$ for 50 years after launch to comply with the COSPAR planetary protection policy (Kminek and Rummel, 2015). We compare our orbit parameters with Suchantke et al. (2020) and conclude that there is a negligible probability of de-orbiting within 50 years.

6. Programmatics

6.1. Cost estimate, descoping options and additional instrumentation

We expect M^5 to be classified as an L-class mission according to the Cosmic Vision strategy of ESA. We have not made detailed cost estimates, but we expect that meeting the cost limit of MEUR 1000 will be challenging. One area for cost reduction, which is not required but may be desirable, is the possibility of collaborating with international partners.

Given the significant cost of the mission, descoping options are possible at the cost of reducing the scientific objectives. From the MFOs, one or more spacecraft could be descoped to lower mass and cost. However, this would significantly hinder the fulfillment of the science objectives, as a 4 spacecraft formation is needed to achieve most science objectives, namely O1.1, O1.2, O1.3, O2.2 (see Table 2). A reduction to 3 spacecraft would reduce the 3D picture to a 2D picture, meaning that boundary orientation and movement could no longer be separated. In addition, the curlometer and wave telescope techniques would only give good scientific return in a limited number of cases. A further reduction to 2 spacecraft would make answering of the science questions even more challenging, reducing the data to a 1D picture.

In the initial, preliminary design presented in this study, all MFOs are designed the same. This reduces cost and adds instrument/measurement redundancy for some instruments. It also provides additional possibilities of scientific observations and adds to spatial resolution and thus increases the scientific value of the overall mission. However, as given by the traceability of the instrument requirements in Table 2, there are possibilities to descope instruments onboard the MFOs without loss of science objectives presented in Table 1, such as two of the electron spectrometers. Additionally, the absence of electric antennas on the MFOs would result in a limited loss of scientific objectives. Instead of descoping, replacement by other instruments could be considered. Some examples of instrumentation that would increase the scientific value of the mission are for example a radiation monitor such as the BepiColombo Environment Radiation Monitor (BERM) (Pinto et al., 2022) or a solar energetic particle detector such as that in the Solar Intensity X-ray and Particle Spectrometer (SIXS) onboard BepiColombo (Huovelin et al., 2020). This would for example assist in monitoring solar eruptive events such as CMEs, which can strongly influence the Martian magnetosphere. Another, but possibly more demanding option in terms of resource allocation, is an Energetic Neutral Atom (ENA) imager. Although ASPERA-3 (Lundin et al., 2004) onboard Mars Express and MINPA (Kong et al., 2020) onboard Tianwen-1 are probing the ENA environment of Mars, open questions still remain (Ramstad et al., 2022). Thus, an ENA imager would improve the understanding of the dynamics of the Martian plasma environment. The addition of any of these instruments without descoping other instruments would however greatly alter the complete mission design and increase cost significantly, as the current system budgets (especially telemetry and propellant) are already at their respective limits. Thus, such additions are not considered in more detail here.

6.2. Mission readiness & risk analysis

All mission components have Technology Readiness Level (TRL) $\geqslant 6$, so there are no significant technological risks to the mission. Some significant operational risks have been identified for the mission. One risk would be if either the communication with the SWO or with one (or more) of the MFO would be lost (resulting in the loss of some science objectives). In the case of losing the SWO, it may be possible to use MRO, MAVEN, or the ExoMars orbiter as a relay instead (Edwards et al., 2014). Another risk would be a failed launch, as well as an error in the orbit insertion, both of which could result in a total loss of the mission. An error in the alignment of the MFO tetrahedron is also a possible risk. The solar panels or the electric antennas not deploying would cause major difficulties for the mission. Using the risk analysis methods outlined in ECSS-M-ST-80C (2008) we believe all of these risks can be classed as either low (1 in 1000 projects) or very low (1 in 10000 projects) risks, and are thus deemed acceptable.

6.3. Outreach

Outreach is a key aspect for scientific space missions. As a scientific community there is a responsibility to inform taxpayers about how their money is being spent on research. Furthermore, outreach is a key driver for inspiring and encouraging young people to consider careers in

Science, Technology, Engineering and Mathematics (STEM). M^5 will therefore have an associated outreach program, designed in accordance with current best practices. This would consist of a pre-launch program of online and in-person events to build excitement, and continue with press releases announcing key science results, and accompanying educational materials for schools, following the model of previous ESA missions (Heck and Madsen, 2003; Lindberg Christensen, 2007).

7. Conclusion

Through detailed preliminary analysis, we show the feasibility of a multi-spacecraft mission to Mars, aiming to extend and complement our understanding of the Martian induced magnetosphere. This understanding will further extend our comprehension of induced magnetospheric systems generally, and of their interaction with the solar wind. Atmospheres are important for the presence of life, and the escape of the Martian one will be better understood by the quantitative characterization of the magnetotail and of the processes taking place there.

In order to study these regions and phenomena on different scales, and in order to separate spatial and temporal variations without having to use imperfect a priori information, a three-dimensional picture of the bow shock, magnetic pile-up boundary as well as the magnetotail are achieved thanks to a four spacecraft configuration. The remaining spacecraft will complement the fleet of solar wind observatories in our solar system, crucial in order to provide better data for space weather applications.

We show the feasibility of these objectives through detailed analyses of the orbital dynamics, formation requirements, and budget constraints such as mass, power and communication. We give an overview of spacecraft design incorporating all critical systems, and show the availability of heritage instruments sufficient to achieve the desired science objectives.

The presented ambitious but feasible mission concept shows that a comprehensive study of the Martian magnetospheric system is possible, which is imperative for future human exploration of Mars. We show that M^5 would greatly advance our understanding of atmospheric escape, and give a crucial reference point for comparative studies of other solar system and exoplanetary induced magnetospheres.

Declaration of Competing Interest

The authors declare that they have no known competing financial interests or personal relationships that could have appeared to influence the work reported in this paper.

Acknowledgments

The authors acknowledge funding from the European Space Agency (ESA) and the Austrian Research Promotion Agency (FFG), which supported Summer School Alpbach 2022, on the theme "Comparative Plasma Physics in the Universe".

We also acknowledge valuable discussions with the tutors of the Summer School Alpbach 2022, Carlos Pintassilgo and Brian Reville.

MB gratefully acknowledges support from the Norwegian Space Agency to attend the Summer School Alpbach 2022.

MB-S and DT gratefully acknowledge the support from the Österreichische Forschungsförderungs GmbH (FFG) for participating in the Summer School Alpbach 2022.

PD gratefully acknowledges funding support from the Centre National d'Études Spatiales (CNES) for participating in the Summer School Alpbach 2022.

ADI gratefully acknowledges support from Agenzia Spaziale Italiana to attend the Summer School Alpbach 2022.

JG and LS gratefully acknowledge funding support from Deutsches Zentrum für Luft- und Raumfahrt for participating in the Summer School Alpbach 2022.

CJKL gratefully acknowledges support from SRON to attend the Summer School Alpbach 2022, and gratefully acknowledges support from the International Max Planck Research School for Astronomy and Cosmic Physics at the University of Heidelberg in the form of an IMPRS PhD fellowship. CJKL gratefully acknowledges further support by the German Deutsche Forschungsgemeinschaft, DFG in the form of an Emmy Noether Research Group – Project-ID 445674056 (SA4064/1–1, PI Sander) and the Federal Ministry of Education and Research (BMBF) and the Baden-Württemberg Ministry of Science as part of the Excellence Strategy of the German Federal and State Governments.

SL and SNÖ gratefully acknowledge support from the Swedish National Space Agency to attend the Summer School Alpbach.

VL gratefully acknowledges the support from the Finnish Centre of Excellence in Research of Sustainable Space (FORESAIL) and the School of Electrical Engineering of Aalto University for participating in the Summer School Alpbach 2022.

References

Abcouwer, N., Daftry, S., del Sesto, T., et al., 2021. Machine learning based path planning for improved rover navigation. In: 2021 IEEE Aerospace Conference (50100), pp. 1–9. https://doi.org/10.1109/AERO50100.2021.9438337.

Acuna, M., Scheifele, J., Stella, P., et al., 1996. Magnetic field cancellation techniques for the mars global surveyor solar array. In: Conference Record of the Twenty Fifth IEEE Photovoltaic Specialists Conference-1996. IEEE, pp. 325–328.

Airapetian, V.S., Barnes, R., Cohen, O., et al., 2020. Impact of space weather on climate and habitability of terrestrial-type exoplanets. Int. J. Astrobiol. 19 (2), 136–194. https://doi.org/10.1017/S1473550419000132.

Angelopoulos, V., 2009. The THEMIS mission. Springer.

Artemyev, A., Angelopoulos, V., Runov, A., et al., 2020. Ionospheric outflow during the substorm growth phase: Themis observations of

oxygen ions at the plasma sheet boundary. J. Geophys. Res.: Space Phys. 125 (7), e2019JA027612.
Auster, H.U., Glassmeier, K.H., Magnes, W., et al., 2008. The themis fluxgate magnetometer. Space Sci. Rev. 141 (1), 235–264. https://doi.org/10.1007/s11214-008-9365-9.
Balogh, A., Dunlop, M., Cowley, S., et al., 1997. The cluster magnetic field investigation. Space Sci. Rev. 79 (1), 65–91.
Brain, D.A., Bagenal, F., Acuña, M.H. et al., 2003. Martian magnetic morphology: Contributions from the solar wind and crust.J. Geophys. Res.: Space Phys., 108(A12). URL: https://agupubs.onlinelibrary.wiley.com/doi/abs/10.1029/2002JA009482. doi: http://dx.doi.org/10.1029/2002JA009482. arXiv:https://agupubs.onlinelibrary.wiley.com/doi/pdf/10.1029/2002JA009482.
Brain, D.A., Bagenal, F., Acuña, M.H., et al., 2002. Observations of low-frequency electromagnetic plasma waves upstream from the Martian shock. J. Geophys. Res.: Space Phys. 107 (A6), SMP 9-1–SMP 9-11. https://doi.org/10.1029/2000JA000416.
Brain, D.A., Baker, A.H., Briggs, J. et al., 2010. Episodic detachment of martian crustal magnetic fields leading to bulk atmospheric plasma escape. Geophys. Res. Lett., 37(14). URL: https://agupubs.onlinelibrary.wiley.com/doi/abs/10.1029/2010GL043916. doi: http://dx.doi.org/10.1029/2010GL043916. arXiv:https://agupubs.onlinelibrary.wiley.com/doi/pdf/10.1029/2010GL043916.
Brain, D.A., McFadden, J., Halekas, J.S., et al., 2015. The spatial distribution of planetary ion fluxes near mars observed by maven. Geophys. Res. Lett. 42 (21), 9142–9148.
Burch, J., Moore, T., Torbert, R., et al., 2016. Magnetospheric multiscale overview and science objectives. Space Sci. Rev. 199, 5–21.
Burch, J., Phan, T., 2016. Magnetic reconnection at the dayside magnetopause: Advances with mms. Geophys. Res. Lett. 43 (16), 8327–8338.
Carr, C., Cupido, E., Lee, C., et al., 2007. Rpc: The rosetta plasma consortium. Space Sci. Rev. 128, 629–647.
Chicarro, A., Martin, P., Trautner, R., 2004. The mars express mission: an overview. Mars Exp.: Scient. Payload 1240, 3–13.
Cucinotta, F.A., Kim, M.-H.Y., Chappell, L.J., et al., 2013. How safe is safe enough? Radiation risk for a human mission to Mars. PloS one 8 (10), e74988.
Curry, S.M., Tatum, P., Mitchell, D., et al., 2022. Ion acceleration in mars' twisted magnetotail. Month. Notices Roy. Astron. Soc.: Lett. 517 (1), L121–L125.
DiBraccio, G.A., Dann, J., Espley, J.R., et al., 2017. MAVEN observations of tail current sheet flapping at Mars. J. Geophys. Res. (Space Phys.) 122 (4), 4308–4324. https://doi.org/10.1002/2016JA023488.
DiBraccio, G.A., Espley, J.R., Gruesbeck, J.R., et al., 2015. Magnetotail dynamics at mars: Initial maven observations. Geophys. Res. Lett. 42 (21), 8828–8837.
Dong, Y., Fang, X., Brain, D., et al., 2015. Strong plume fluxes at mars observed by maven: An important planetary ion escape channel. Geophys. Res. Lett. 42 (21), 8942–8950.
Dubinin, E., Fraenz, M., 2015. Magnetotails of Mars and Venus. Magnetotails in the solar system 207, 34–59.
Dubinin, E., Fraenz, M., Pätzold, M., et al., 2017. The effect of solar wind variations on the escape of oxygen ions from mars through different channels: Maven observations. J. Geophys. Res.: Space Phys. 122 (11), 11–285.
Dubinin, E., Fraenz, M., Pätzold, M. et al., 2020. Impact of martian crustal magnetic field on the ion escape.J. Geophys. Res.: Space Phys., 125(10), e2020JA028010. URL: https://agupubs.onlinelibrary.wiley.com/doi/abs/10.1029/2020JA028010. doi: http://dx.doi.org/10.1029/2020JA028010. arXiv:https://agupubs.onlinelibrary.wiley.com/doi/pdf/10.1029/2020JA028010. E2020JA028010 10.1029/2020JA028010.
Dunlop, M., Southwood, D., Glassmeier, K.-H., et al., 1988. Analysis of multipoint magnetometer data. Adv. Space Res. 8 (9), 273–277. https://doi.org/10.1016/0273-1177(88)90141-X.
Dunlop, M.W., Dong, X.-C., Wang, T.-Y., et al., 2021. Curlometer technique and applications. J. Geophys. Res.: Space Phys. 126 (11), e2021JA029538.
Eastwood, J.P., Brain, D.A., Halekas, J.S., et al., 2008. Evidence for collisionless magnetic reconnection at Mars. Geophys. Res. Lett. 35 (2).
ECSS-M-ST-80C, 2008. Risk management. Standard European Cooperation for Space Standardization Noordwijk, NL.
ECSS-U-ST-20C, 2019. Planetary protection. Standard European Cooperation for Space Standardization Noordwijk, NL.
Edwards, C.D., Barela, P.R., Gladden, R.E., et al., 2014. Replenishing the mars relay network. In: 2014 IEEE Aerospace Conference. IEEE, pp. 1–13.
Ergun, R.E., Andersson, L.A., Fowler, C.M., et al., 2021. In-Situ Measurements of Electron Temperature and Density in Mars' Dayside Ionosphere. Geophys. Res. Lett. 48 (14). https://doi.org/10.1029/2021GL093623, e2021GL093623.
ESA, 2014. Margin Philosophy for Science Assessment Studies. ESA (2nd ed.).
Escoubet, C.P., Masson, A., Laakso, H., et al., 2021. Cluster after 20 years of operations: Science highlights and technical challenges. J. Geophys. Res.: Space Phys. 126 (8). https://doi.org/10.1029/2021JA029474, e2021JA029474.
Escoubet, C.P., Schmidt, R., Goldstein, M.L., 1997. Cluster – science and mission overview. Space Sci. Rev. 79 (1), 11–32. https://doi.org/10.1023/A:1004923124586.
Fang, X., Ma, Y., Masunaga, K. et al., 2017. The mars crustal magnetic field control of plasma boundary locations and atmospheric loss: Mhd prediction and comparison with maven.J. Geophys. Res.: Space Phys., 122(4), 4117–4137. URL: https://agupubs.onlinelibrary.wiley.com/doi/abs/10.1002/2016JA023509. doi: https://doi.org/10.1002/2016JA023509. arXiv: https://agupubs.onlinelibrary.wiley.com/doi/pdf/10.1002/2016JA023509.
Graf, J.E., Zurek, R.W., Eisen, H.J., et al., 2005. The Mars reconnaissance orbiter mission. Acta Astronaut. 57 (2), 566–578. https://doi.org/10.1016/j.actaastro.2005.03.043.
Gunell, Herbert, Maggiolo, Romain, Nilsson, Hans et al., 2018. Why an intrinsic magnetic field does not protect a planet against atmospheric escape. A&A, 614, L3. URL: https://doi.org/10.1051/0004-6361/201832934. doi:10.1051/0004-6361/201832934.
Gustafsson, G., Boström, R., Holback, B., et al., 1997. The electric field and wave experiment for the cluster mission. Space Sci. Rev. 79 (1), 137–156. https://doi.org/10.1023/A:1004975108657.
Götz, C., Gunell, H., Volwerk, M., et al., 2019. Cometary Plasma Science – A White Paper in response to the. In: Voyage 2050 Call by the European Space Agency. https://doi.org/10.48550/ARXIV.1908.00377.
Haaland, S., Runov, A., Artemyev, A., et al., 2019. Characteristics of the flank magnetopause: Themis observations. J. Geophys. Res.: Space Phys. 124 (5), 3421–3435.
Hanaoka, Y., Watanabe, K., Yashiro, S., 2023. Origin of solar storms. In: Solar-Terrestrial Environmental Prediction. Springer, pp. 251–287.
Harada, Y., Halekas, J.S., McFadden, J.P., et al., 2015. Marsward and tailward ions in the near-Mars magnetotail: MAVEN observations. Geophys. Res. Lett. 42 (21), 8925–8932. https://doi.org/10.1002/2015GL065005.
Hassler, D.M., Zeitlin, C., Ehresmann, B., et al., 2018. Space weather on the surface of Mars: Impact of the September 2017 Events. Space Weather 16 (11), 1702–1708. https://doi.org/10.1029/2018SW001959.
Heck, A., Madsen, C., 2003. Astronomy Communication. Springer Science & Business Media.
Hesse, M., Liu, Y.-H., Chen, L.-J., et al., 2016. On the electron diffusion region in asymmetric reconnection with a guide magnetic field. Geophys. Res. Lett. 43 (6), 2359–2364.
Holmberg, M.K.G., André, N., Garnier, P., et al., 2019. MAVEN and MEX Multi-instrument Study of the Dayside of the Martian Induced Magnetospheric Structure Revealed by Pressure Analyses. J. Geophys. Res.: Space Phys. 124 (11), 8564–8589. https://doi.org/10.1029/2019JA026954.
Huovelin, J., Vainio, R., Kilpua, E., et al., 2020. Solar intensity x-ray and particle spectrometer sixs: Instrument design and first results. Space Sci. Rev. 216 (5), 94. https://doi.org/10.1007/s11214-020-00717-3.

Jakosky, B., Brain, D., Chaffin, M. et al., 2018. Loss of the martian atmosphere to space: Present-day loss rates determined from maven observations and integrated loss through time. Icarus, 315, 146–157. URL: https://www.sciencedirect.com/science/article/pii/S0019103517306917. doi: http://dx.doi.org/10.1016/j.icarus.2018.05.030.

Jakosky, B.M., Lin, R.P., Grebowsky, J.M., et al., 2015. The Mars atmosphere and volatile evolution (MAVEN) Mission. Space Sci. Rev. 195 (1), 3–48. https://doi.org/10.1007/s11214-015-0139-x.

Jakosky, B.M., Slipski, M., Benna, M., et al., 2017. Mars' atmospheric history derived from upper-atmosphere measurements of 38ar/36ar. Science 355 (6332), 1408–1410. https://doi.org/10.1126/science.aai7721.

Jesick, M., Demcak, S., Young, B., et al., 2017. Navigation overview for the mars atmosphere and volatile evolution mission. J. Spacecraft Rock. 54 (1), 29–43.

Karlsson, T., Marklund, G.T., Figueiredo, S., et al., 2004. Separating spatial and temporal variations in auroral electric and magnetic fields by Cluster multipoint measurements. Ann. Geophys. 22 (7), 2463–2472.

Kminek, G., Rummel, J.D., 2015. Cospar's planetary protection policy. Space Res. Today 193, 7–19.

Kong, L., Zhang, A., Tian, Z. et al., 2020. Mars ion and neutral particle analyzer (minpa) for chinese mars exploration mission (tianwen-1): Design and ground calibration. Earth and Planetary Physics, 4(4), 333–344. URL: https://www.eppcgs.org/en/article/doi/10.26464/epp2020053. doi:10.26464/epp2020053.

Kuramoto, K., Kawakatsu, Y., Fujimoto, M., et al., 2022. Martian moons exploration mmx: sample return mission to phobos elucidating formation processes of habitable planets. Earth, Planets and Space 74 (1), 1–31.

Langlais, B., Thébault, E., Houliez, A. et al., 2019. A new model of the crustal magnetic field of mars using mgs and maven. J. Geophys. Res.: Planets, 124(6), 1542–1569. URL: https://agupubs.onlinelibrary.wiley.com/doi/abs/10.1029/2018JE005854. doi: http://dx.doi.org/10.1029/2018JE005854. arXiv: https://agupubs.onlinelibrary.wiley.com/doi/pdf/10.1029/2018JE005854.

Li, W., Raeder, J., Øieroset, M., et al., 2009. Cold dense magnetopause boundary layer under northward imf: Results from themis and mhd simulations. J. Geophys. Res.: Space Phys. 114 (A1).

Lillis, R.J., Curry, S.M., Ma, Y.J. et al., 2022. ESCAPADE: A Twin-Spacecraft Simplex Mission to Unveil Mars' Unique Hybrid Magnetosphere. In LPI Contributions (p. 1135). volume 2678 of LPI Contributions.

Lillis, R.J., Mitchell, D., Montabone, L., et al., 2021. Mosaic: A satellite constellation to enable groundbreaking mars climate system science and prepare for human exploration. Planet. Sci. J. 2 (5), 211.

Lin, R.T., Huang, S.Y., Yuan, Z.G., et al., 2021. Characteristics of Energetic Oxygen Ions Escaping From Mars: MAVEN Observations. J. Geophys. Res. (Space Phys.) 126 (8), e29507. https://doi.org/10.1029/2021JA029507.

Lindberg Christensen, L., 2007. The Hands-On Guide for Science Communicators: A Step-by-Step Approach to Public Outreach. Springer, New York.

Lundin, R., Barabash, S., Andersson, H., et al., 2004. Solar wind-induced atmospheric erosion at mars: First results from aspera-3 on mars express. Science 305 (5692), 1933–1936. https://doi.org/10.1126/science.1101860, URL: https://www.science.org/doi/abs/10.1126/science.1101860. arXiv:https://www.science.org/doi/pdf/10.1126/science.1101860.

Ma, Y., Fang, X., Russell, C.T. et al., 2014. Effects of crustal field rotation on the solar wind plasma interaction with mars. Geophys. Res. Lett., 41(19), 6563–6569. URL: https://agupubs.onlinelibrary.wiley.com/doi/abs/10.1002/2014GL060785. doi: http://dx.doi.org/10.1002/2014GL060785. arXiv:https://agupubs.onlinelibrary.wiley.com/doi/pdf/10.1002/2014GL060785.

Ma, Y., Russell, C.T., Toth, G., et al., 2018. Reconnection in the Martian Magnetotail: Hall-MHD With Embedded Particle-in-Cell Simulations. J. Geophys. Res. (Space Phys.) 123 (5), 3742–3763. https://doi.org/10.1029/2017JA024729.

Marusek, J.A., 2007. Solar storm threat analysis. J. Marusek.

Matsunaga, K., Seki, K., Brain, D.A., et al., 2017. Statistical study of relations between the induced magnetosphere, ion composition, and pressure balance boundaries around Mars Based On MAVEN Observations. J. Geophys. Res.: Space Phys. 122 (9), 9723–9737. https://doi.org/10.1002/2017JA024217.

McFadden, J., Carlson, C., Larson, D., et al., 2009. Themis esa first science results and performance issues. The THEMIS mission, pp. 477–508.

Motschmann, U., Woodward, T.I., Glassmeier, K.H., et al., 1996. Wavelength and direction filtering by magnetic measurements at satellite arrays: Generalized minimum variance analysis. J. Geophys. Res.: Space Phys. 101 (A3), 4961–4965. https://doi.org/10.1029/95JA03471.

Narita, Y., Glassmeier, K., Motschmann, U., 2010. Wave vector analysis methods using multi-point measurements. Nonlinear Process. Geophys. 17, 383–394.

Narita, Y., Glassmeier, K.-H., Motschmann, U., 2022. The wave telescope technique. J. Geophys. Res.: Space Phys. 127 (2). https://doi.org/10.1029/2021JA030165, e2021JA030165.

Nilsson, H., Lundin, R., Lundin, K., et al., 2007. RPC-ICA: The ion composition analyzer of the Rosetta Plasma Consortium. Space Sci. Rev. 128 (1), 671–695.

Nilsson, H., Stenberg, G., Futaana, Y., et al., 2012. Ion distributions in the vicinity of Mars: Signatures of heating and acceleration processes. Earth, Planets Space 64 (2), 9. https://doi.org/10.5047/eps.2011.04.011.

Owen, C.J., Bruno, R., Livi, S. et al., 2020. The solar orbiter solar wind analyser (SWA) suite. Astron. Astrophys., 642, A16.

Pavón, S., Tregubow, V., Peukert, M. et al., 2012. Engineering validation model for the exomars bi-propellant propulsion subsystem. In SP2012_2353312, European Space Propulsion Conference Bordeaux.

Pinto, M., Sanchez-Cano, B., Moissl, R., et al., 2022. The bepicolombo environment radiation monitor, berm. Space Sci. Rev. 218 (7), 54. https://doi.org/10.1007/s11214-022-00922-2.

Přech, L., Němeček, Z., Šafránková, J., 2008. Response of magnetospheric boundaries to the interplanetary shock: Themis contribution. Geophys. Res. Lett. 35 (17).

Ramstad, R., Barabash, S., 2021. Do intrinsic magnetic fields protect planetary atmospheres from stellar winds? lessons from ion measurements at mars, venus, and earth. Space Sci. Rev. 217, 1–39.

Ramstad, R., Brain, D.A., Dong, Y., et al., 2020. The global current systems of the Martian induced magnetosphere. Nat. Astron. 4 (10), 979–985. https://doi.org/10.1038/s41550-020-1099-y.

Ramstad, R., Brain, D.A., Dong, Y., et al., 2022. Energetic neutral atoms near mars: Predicted distributions based on maven measurements. Astrophys J 927 (1), 11. https://doi.org/10.3847/1538-4357/ac4606.

Sakata, R., Seki, K., Sakai, S. et al., 2020. Effects of an intrinsic magnetic field on ion loss from ancient mars based on multispecies mhd simulations.J. Geophys. Res.: Space Phys., 125(2), e2019JA026945. URL: https://agupubs.onlinelibrary.wiley.com/doi/abs/10.1029/2019JA026945. doi: http://dx.doi.org/10.1029/2019JA026945. arXiv: https://agupubs.onlinelibrary.wiley.com/doi/pdf/10.1029/2019JA026945. E2019JA026945 2019JA026945.

Sánchez-Cano, B., Lester, M., Andrews, D.J. et al., 2021. Mars' plasma system. Scientific potential of coordinated multipoint missions: "The next generation". Experimental Astronomy, doi:10.1007/s10686-021-09790-0.

Sanchez-Cano, B., Opgenoorth, H., Leblanc, F. et al., 2022. The M-MATISSE mission: Mars Magnetosphere ATmosphere Ionosphere and Surface SciencE. In: 44th COSPAR Scientific Assembly. Held 16–24 July (p. 421). volume 44.

Shay, M., Phan, T., Haggerty, C., et al., 2016. Kinetic signatures of the region surrounding the x line in asymmetric (magnetopause) reconnection. Geophys. Res. Lett. 43 (9), 4145–4154.

Sibeck, D., Angelopoulos, V., 2008. Themis science objectives and mission phases. Space Sci. Rev. 141, 35–59.

Suchantke, I., Letizia, F., Braun, V. et al., 2020. Space sustainability in martian orbits — first insights in a technical and regulatory analysis. J. Space Saf. Eng., 7(3), 439–446. URL: https://www.sciencedirect.com/science/article/pii/S2468896720300677. doi: http://dx.doi.org/10.1016/j.jsse.2020.07.003. Space Debris: The State of Art.

Thomas, V.C., Makowski, J.M., Brown, G.M., et al., 2011. The dawn spacecraft. Space Sci. Rev. 163 (1), 175–249. https://doi.org/10.1007/s11214-011-9852-2.

Trotignon, J., Mazelle, C., Bertucci, C., et al., 2006. Martian shock and magnetic pile-up boundary positions and shapes determined from the Phobos 2 and Mars Global Surveyor data sets. Planet. Space Sci. 54 (4), 357–369. https://doi.org/10.1016/j.pss.2006.01.003.

Voyage 2050 Senior Committee (2021). Voyage 2050 Final Recommendations.

Wang, J., Yu, J., Xu, X., et al., 2021. MAVEN observations of magnetic reconnection at martian induced magnetopause. Geophys. Res. Lett. 48 (21), e95426. https://doi.org/10.1029/2021GL095426.

Welch, R., Limonadi, D., Manning, R., 2013. Systems engineering the Curiosity Rover: A retrospective. In: 2013 8th International Conference on System of Systems Engineering, pp. 70–75. https://doi.org/10.1109/SYSoSE.2013.6575245.

Yadav, V.K., 2021. Plasma waves around Venus and Mars. IETE Tech. Rev. 38 (6), 622–661. https://doi.org/10.1080/02564602.2020.1819889.

Yasaka, T., Onoda, J., 2003. Spacecraft structures. In: Meyers, R.A. (Ed.), Encyclopedia of Physical Science and Technology (Third Edition). New York: Academic Press. (Third edition ed.), pp. 449–461. doi: http://dx.doi.org/10.1016/B0-12-227410-5/00899-1.

Zou, Y., Zhu, Y., Bai, Y., et al., 2021. Scientific objectives and payloads of tianwen-1, China's first Mars exploration mission. Adv. Space Res. 67 (2), 812–823.